JCB Journal of Cell Biology

ARTICLE

Chromosome oscillation promotes Aurora A–dependent Hec1 phosphorylation and mitotic fidelity

Kenji Iemura[1], Toyoaki Natsume[2,3], Kayoko Maehara[4], Masato T. Kanemaki[2,3], and Kozo Tanaka[1]

Most cancer cells show chromosomal instability, a condition where chromosome missegregation occurs frequently. We found that chromosome oscillation, an iterative chromosome motion during metaphase, is attenuated in cancer cell lines. We also found that metaphase phosphorylation of Hec1 at serine 55, which is mainly dependent on Aurora A on the spindle, is reduced in cancer cell lines. The Aurora A–dependent Hec1-S55 phosphorylation level was regulated by the chromosome oscillation amplitude and vice versa: Hec1-S55 and -S69 phosphorylation by Aurora A is required for efficient chromosome oscillation. Furthermore, enhancement of chromosome oscillation reduced the number of erroneous kinetochore–microtubule attachments and chromosome missegregation, whereas inhibition of Aurora A during metaphase increased such errors. We propose that Aurora A–mediated metaphase Hec1-S55 phosphorylation through chromosome oscillation, together with Hec1-S69 phosphorylation, ensures mitotic fidelity by eliminating erroneous kinetochore–microtubule attachments. Attenuated chromosome oscillation and the resulting reduced Hec1-S55 phosphorylation may be a cause of CIN in cancer cell lines.

Introduction

Most cancer cells have an abnormal number of chromosomes, known as aneuploidy (Ben-David and Amon, 2020; Weaver and Cleveland, 2006). Aneuploidy in cancer cells usually results from chromosomal instability (CIN), a condition in which chromosome missegregation occurs at a high rate (Bakhoum and Compton, 2012a; Gordon et al., 2012; Tanaka and Hirota, 2016). Aneuploidy caused by CIN is generally disruptive to cellular fitness, but the resultant genetic heterogeneity is supposed to promote tumor formation and progression through clonal selection of any cells that acquire growth advantage. For proper chromosome segregation, kinetochores on the sister chromatids of replicated chromosomes must attach to microtubules from opposite spindle poles, referred to as amphitelic attachment or bi-orientation (Tanaka, 2013; Tanaka et al., 2005). The spindle assembly checkpoint (SAC) and the error correction mechanism ensure bi-orientation establishment for all chromosomes: the SAC delays anaphase onset in the presence of unattached kinetochores, while Aurora kinases are involved in the correction of erroneous attachments, such as monotelic, syntelic, and merotelic attachment (Godek et al., 2015; Tanaka, 2002). Among these, merotelic attachment, in which a single kinetochore attaches to microtubules from both spindle poles, is not detected by the SAC and is thus considered as a main cause of CIN (Cimini, 2008). Conditions such as increased formation of merotelic attachment due to centrosome amplification and reduced correction of merotelic attachment due to microtubule stabilization or reduced Aurora B activity have been proposed to induce CIN in cancer cells (Holland and Cleveland, 2012; Tanaka and Hirota, 2016), although the underlying causes are not fully understood.

Correction of the erroneous kinetochore–microtubule attachments by Aurora kinases is mainly performed by phosphorylation of Hec1, a component of the Ndc80 complex that is involved in the attachment of kinetochores to microtubules (DeLuca et al., 2006). It has been shown that phosphorylation of the N-terminal tail of Hec1 reduces the affinity of the Ndc80 complex to microtubules and destabilizes kinetochore–microtubule attachments, facilitating the error correction (Wimbish and DeLuca, 2020; Zaytsev et al., 2014). Aurora B, which is mainly detected at inner centromere, plays a major role in the error correction (Cimini et al., 2006; Lampson and Cheeseman, 2011), whereas Aurora A, which resides on the

[1]Department of Molecular Oncology, Institute of Development, Aging and Cancer, Tohoku University, Sendai, Miyagi, Japan; [2]Department of Chromosome Science, National Institute of Genetics, Research Organization of Information and Systems, Mishima, Shizuoka, Japan; [3]Department of Genetics, The Graduate University for Advanced Studies, Mishima, Shizuoka, Japan; [4]Department of Nutrition, Graduate School of Health Sciences, Kio University, Kitakatsuragi, Nara, Japan.

Correspondence to Kozo Tanaka: kozo.tanaka.d2@tohoku.ac.jp.

spindle particularly at the poles, is known to phosphorylate Hec1 when chromosomes are near spindle poles (Chmátal et al., 2015; Ye et al., 2015). Interestingly, recent works have shown that Aurora A phosphorylates Hec1 at serine 69 (Hec1-S69) not only during prometaphase but also during metaphase, when chromosomes are aligned at the spindle equator distant from spindle poles (Bucko et al., 2019; DeLuca et al., 2018).

During metaphase in mammalian cells, kinetochore pairs repeatedly move around the spindle equator, known as chromosome oscillation (Jaqaman et al., 2010; Skibbens et al., 1993; Wan et al., 2012), but the physiological roles of such oscillation remain elusive. We found that chromosome oscillation is attenuated in cancer cell lines, and this is correlated with reduced Hec1 phosphorylation at serine 55 (Hec1-S55) during metaphase. Furthermore, a fraction of Aurora A residing at the spindle is mainly responsible for the metaphase Hec1-S55 phosphorylation. Intriguingly, the Hec1-S55 phosphorylation, together with phosphorylation at Hec1-S69, promotes chromosome oscillation and contributes to the correction of erroneous kinetochore–microtubule attachments, thus ensuring faithful chromosome segregation. Our data suggest that reduction of the metaphase Hec1-S55 phosphorylation by Aurora A due to attenuated chromosome oscillation is one of the causes of CIN in cancer cell lines.

Results

Chromosome oscillation is attenuated in cancer cell lines

First, we compared chromosome oscillation in human retinal pigment epithelial (RPE-1) cells, a nontransformed cell line, and the HeLa cancer cell line. When cells were arrested in metaphase by treatment with MG132, a proteasome inhibitor that prohibits progression from metaphase to anaphase, the amplitude of oscillation was bigger in RPE-1 cells than in HeLa cells (Fig. 1, A and B and Video 1). We confirmed that amplitude of chromosome oscillation is comparable in the presence or absence of MG132 (Fig. S1, A and B and Video 2). We also observed chromosome oscillation in other nontransformed (TIG-3) and cancer cell lines (HCT-15, DLD-1, HCT116, DU145, A549, U2OS, and MCF-7) and found a general tendency that chromosome oscillation is reduced in cancer cell lines (Fig. 1 C and Video 3). The reduced amplitude of chromosome oscillation in cancer cell lines was determined by quantifying the deviation from average position (DAP; Stumpff et al., 2008) for tracked kinetochores, which was higher in nontransformed cell lines compared with cancer cell lines (Fig. 1 D). Interestingly, the amplitude of chromosome oscillation in cancer cell lines categorized as "non-CIN" (HCT-15, DLD-1, and HCT116), which show lower rates of micronucleation and karyotypic diversity compared with CIN cell lines (HeLa, DU145, A549, U2OS, and MCF-7; Fig. S1, C and D), was between that of nontransformed cell lines and CIN cell lines (Fig. 1, C and D). We also examined kinetochore distribution during metaphase in fixed cells by quantifying the variance of distance between kinetochores and the spindle equator, finding that it was smaller in cancer cell lines compared with nontransformed cell lines (Fig. S1, E–G). These data suggest that reduced chromosome oscillation is a property of cancer cell lines. There was no general trend distinguishing cancer cell lines from nontransformed cell lines with regard to the difference in spindle length, cell size, and distance between sister kinetochores (Fig. S1, H–J), thus excluding the possibility that these factors are responsible for the reduced chromosome oscillation observed in cancer cell lines.

Phosphorylation of Hec1-S55 during metaphase, which is mediated by Aurora A, is reduced in cancer cell lines

Hec1 phosphorylation at the N-terminal tail, which is mediated by Aurora kinases, is known to reduce the affinity between the Ndc80 complex and microtubules, facilitating the correction of erroneous kinetochore–microtubule attachments (Zaytsev et al., 2014). When we observed phosphorylation of Hec1 at S55 (Hec1-S55) in HeLa cells, it was detected in prometaphase cells but was barely detectable in metaphase cells (Fig. 2, A and B), as previously reported (DeLuca et al., 2011). In RPE-1 cells, by contrast, Hec1-S55 phosphorylation signal in metaphase was detectable at the edge of the metaphase plate, although it was weaker than that in prometaphase (Fig. 2, A and B). We confirmed the specificity of the phospho-Hec1-S55 signal in metaphase by observing the disappearance of the signal in the presence of a blocking peptide (Fig. S2, A and B) and by Hec1 RNAi, which was recovered by expressing WT Hec1, but not by a Hec1 mutant in which S55 was mutated to alanine (Hec1-S55A; DeLuca et al., 2018; Fig. S2, C and D). Treating cells with the phosphatase inhibitor Calyculin A (Ishihara et al., 1989) resulted in increased metaphase Hec1-S55 phosphorylation in RPE-1 cells, consistent with the idea that the Hec1 phosphorylation is counteracted by phosphatase activity (Smith et al., 2019; Fig. S2, E and F). Intriguingly, Calyculin A treatment increased Hec1-S55 phosphorylation signals to detectable levels even in HeLa cells, and this was also prominent at the edge of the metaphase plate (Fig. S2, G and H).

To examine whether the Hec1-S55 phosphorylation during metaphase in RPE-1 cells depends on Aurora B, a major kinase for Hec1 phosphorylation (Cimini et al., 2006; Lampson and Cheeseman, 2011), we treated metaphase-arrested RPE-1 cells with the Aurora B inhibitor AZD1152 (Mortlock et al., 2007). However, the Hec1-S55 phosphorylation signal was not reduced upon AZD1152 treatment (Fig. 2, C and D). In contrast, when we treated metaphase-arrested RPE-1 cells with MLN8237, an Aurora A inhibitor (Hoar et al., 2007; Manfredi et al., 2007), the Hec1-S55 phosphorylation signal was markedly reduced (Fig. 2, C and D), indicating that the Hec1-S55 phosphorylation during metaphase in RPE-1 cells is dependent on Aurora A but not on Aurora B. The Hec1-S55 phosphorylation was also reduced in Calyculin A–treated RPE-1 cells as well as in HeLa cells in the presence of MLN8237 (Fig. S2, E–H), further confirming that Aurora A is the main kinase responsible for the metaphase Hec1-S55 phosphorylation. We examined the metaphase Hec1-S55 phosphorylation level in various cell lines to see whether it is commonly reduced in cancer cells. As shown in Fig. 2, E and F, the metaphase Hec1-S55 phosphorylation level in cancer-derived cell lines was lower compared with that in nontransformed cell lines. Again, non-CIN cancer cell lines showed a higher level of Hec1-S55 phosphorylation compared with CIN

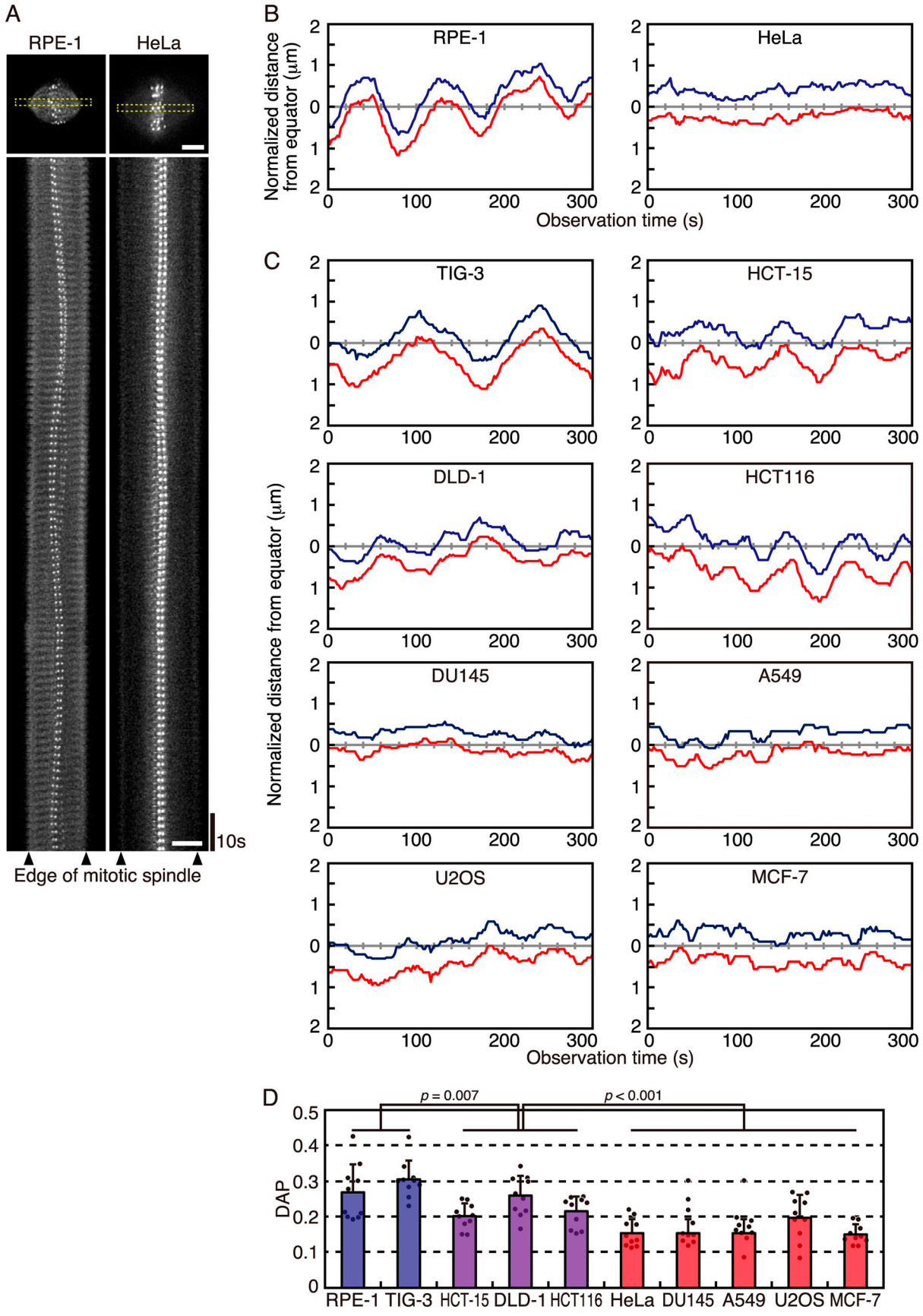

Figure 1. **Chromosome oscillation is attenuated in cancer cell lines. (A)** Kymographs of kinetochore pairs in RPE-1 and HeLa cells expressing EGFP–CENP-A and EGFP–α-tubulin. Cells were arrested in metaphase by MG132 treatment for 2 h and observed by live-cell imaging. Boxed areas in the upper panels were

aligned along the time course. Horizontal scale bar: 5 µm. Vertical scale bar: 10 s. See also Video 1. **(B and C)** Trajectories of kinetochores in RPE-1 and HeLa cells (B) or other nontransformed and cancer cell lines (C) arrested in metaphase. Cells were treated as in A and observed by live-cell imaging. The blue and red trajectories show the movements of a pair of sister kinetochores plotted as the distance from the spindle equator. See also Video 3. **(D)** DAP measurements (Stumpff et al., 2008) of kinetochore position in nontransformed (blue), non-CIN (purple), and CIN (red) cancer cell lines treated as in A. Error bars represent SD of 10 kinetochore pairs from three cells. P values were obtained using the Tukey–Kramer multiple comparisons test.

cancer cell lines (Fig. 2, E and F). Collectively, our data suggest that Hec1-S55 is phosphorylated by Aurora A during metaphase and the phosphorylation is reduced in cancer cell lines.

The phosphorylation of Hec1 at S69 (Hec1-S69) during metaphase was recently reported (DeLuca et al., 2018). We confirmed that Hec1-S69 is phosphorylated in both HeLa and RPE-1 cells during metaphase to levels comparable to those in prometaphase (Fig. S2, I and J), in contrast to Hec1-S55 phosphorylation levels. We further examined the metaphase Hec1-S69 phosphorylation in various cell lines and found Hec1-S69 is phosphorylated at detectable levels both in nontransformed and cancer cell lines (Fig. S2, K and L), thus displaying a sharp contrast to the pattern of Hec1-S55 phosphorylation.

Aurora A residing at the spindle is mainly responsible for Hec1-S55 phosphorylation during metaphase

To confirm the dependency of the metaphase Hec1-S55 phosphorylation on Aurora A, we depleted Aurora A using the auxin-inducible degron (AID) system (Nishimura et al., 2009). We integrated the mini-AID (mAID)–mClover tag into the endogenous Aurora A loci in RPE-1 cells using the CRISPR/Cas9 system (Fig. 3 A; Natsume et al., 2016). Aurora A–mAID-mClover was detected mainly at spindle poles, as expected (Fig. 3 B). These cells were arrested in metaphase by inhibiting anaphase promoting complex/cyclosome with proTAME (Zeng et al., 2010) and apcin (Sackton et al., 2014), as the usual arresting treatment, MG132, inhibits the desired degradation of Aurora A–mAID-mClover. Background auxin activity was suppressed by auxinole (Yesbolatova et al., 2019; Fig. S3 A). When cells were treated with indole-3-acetic acid (IAA), a major auxin species, Aurora A–mAID-mClover was depleted, determined by immunoblot analysis and fluorescence microscopy (Fig. 3 B and Fig. S3 B). In the presence of IAA, the Hec1-S55 phosphorylation signal was reduced (Fig. 3, C and D), confirming that Aurora A is responsible for the Hec1-S55 phosphorylation during metaphase. Treatment with MLN8237 did not reduce the Hec1-S55 phosphorylation signal further, as expected (Fig. 3, C and D). We also depleted Aurora B using the AID system in RPE-1 cells (Fig. S3 C). Aurora B–mAID-mClover was mainly detected at inner centromeres (Fig. S3 D) in cells arrested in metaphase by proTAME/apcin treatment, and this was reduced in the presence of IAA (Fig. S3, B and D). In the presence of IAA, the Hec1-S55 phosphorylation signal was not reduced; it was reduced by MLN8237, but not by AZD1152, confirming that Hec1-S55 phosphorylation is dependent on Aurora A, not on Aurora B (Fig. S3, E and F).

Aurora A is known to localize mainly at spindle poles, and it has been shown to phosphorylate Hec1 on kinetochores in prometaphase when chromosomes are near spindle poles (Chmátal et al., 2015; Ye et al., 2015). However, in metaphase, kinetochores on the metaphase plate are distant from spindle poles; how then does Aurora A phosphorylate Hec1 during metaphase? Recent data suggest that a fraction of Aurora A localizes at the centromere through INCENP, and this fraction is responsible for metaphase Hec1-S69 phosphorylation (DeLuca et al., 2018). To address whether metaphase Hec1-S55 phosphorylation is also mediated by Aurora A at the centromere, we examined the phosphorylation in RPE-1 cells depleted of INCENP (Fig. S3 G). The metaphase phosphorylation level of Hec1-S55 did not decrease upon INCENP depletion, while that of Hec1-S69 was reduced (Fig. S3, H and I), suggesting that the Hec1-S55 phosphorylation during metaphase is not dependent on Aurora A localizing to the centromere through INCENP, unlike Hec1-S69 phosphorylation. As shown in Fig. 2 A, the Hec1-S55 phosphorylation in RPE-1 cells during metaphase was preferentially detected on kinetochores at the edge of the metaphase plate. We validated this tendency by measuring the kinetochore to spindle pole distance in metaphase-arrested RPE-1 cells, depending on the presence or absence of the Hec1-S55 phosphorylation signal (Fig. 3 E). This distance was significantly shorter for kinetochores positive for the Hec1-S55 phosphorylation signal (Fig. 3 E), showing that kinetochores closer to spindle poles are preferentially phosphorylated. We also plotted the intensity of the Hec1-S55 phosphorylation signal on kinetochores along the spindle axis in metaphase-arrested RPE-1 cells expressing Aurora A–mAID-mClover, confirming that Hec1-S55 phosphorylation was higher on kinetochores at the edge of the metaphase plate (Fig. 3 F). In contrast, the Hec1-S69 phosphorylation signal on kinetochores was constant along the metaphase plate (Fig. 3 G). There was a gradient of the Aurora A signal along the spindle axis, from spindle poles to the equator (Fig. 3, F and G), implying that Aurora A phosphorylates Hec1-S55 through an activity gradient, as has been previously suggested (Chmátal et al., 2015; Ye et al., 2015).

Aurora A localizes to the spindle via interaction with TPX2 (Kufer et al., 2002). To specifically explore the contribution of Aurora A residing at the spindle, we observed Hec1-S55 phosphorylation when Aurora A cannot localize to the spindle. We established RPE-1 cells containing an mAID-mClover tag at the endogenous TPX2 loci (Fig. S4 A) and depleted TPX2 in cells arrested in metaphase (Fig. S4, B and C). Cells maintained spindle bipolarity in this condition. As TPX2 is required not only for Aurora A localization to the spindle but also for Aurora A activation (Eyers et al., 2003; Tsai et al., 2003), we expressed a TPX2 construct that contains mutations in the three residues (F307, F334, and H335) at the interfaces between tubulin dimers, which abolish microtubule binding (Zhang et al., 2017). We found the mutant (mCherry-TPX2-3E) does not localize to the spindle, in contrast to WT mCherry-TPX2 but still localizes to spindle poles, supposedly through interaction with other proteins (Fig. 3 H). Accordingly, Aurora A localization on the

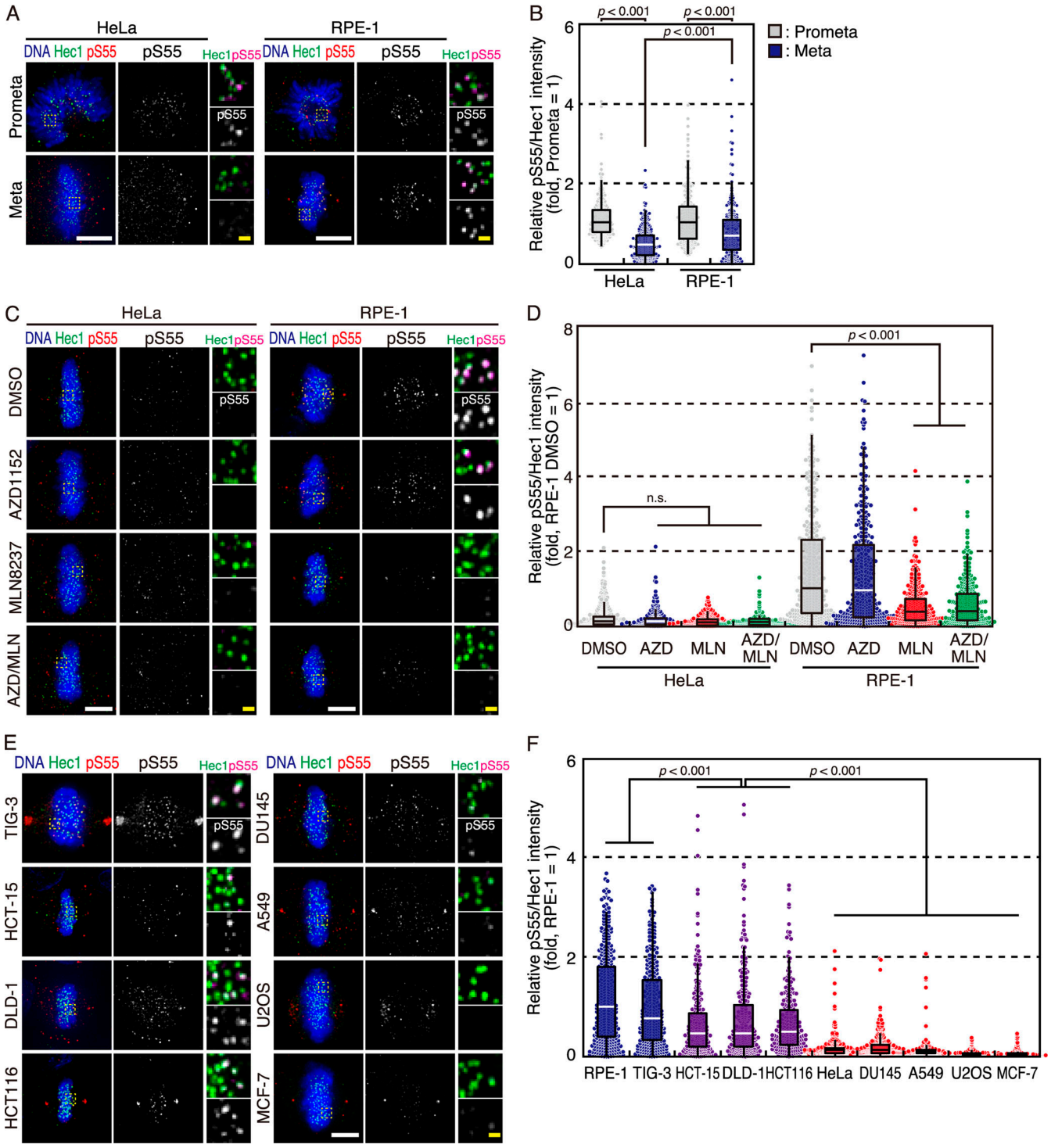

Figure 2. **Hec1-S55 is phosphorylated during metaphase by Aurora A, which is reduced in cancer cell lines. (A)** Hec1-S55 phosphorylation in HeLa and RPE-1 cells during prometaphase (Prometa) and metaphase (Meta). Cells were fixed and stained with anti-Hec1 (green) and anti–phospho-Hec1-S55 (red) antibodies. DNA was stained with DAPI (blue). Boxed regions in the panels are shown as magnified images in insets. Scale bars: 5 µm (white), 500 nm (yellow). **(B)** Quantification of phospho–Hec1-S55 signal in HeLa and RPE-1 cells during prometaphase and metaphase. Relative intensity of the phosphorylated Hec1-S55 signal in cells treated as in A, which was calculated by dividing the phosphorylation signal with Hec1 signal on each kinetochore, displayed as box and dot plots. The bottom and top of the box show the lower and upper quartile values, respectively. The median is indicated with a bar in the box, and the whiskers denote the range within 1.5× size of the box. The median of prometaphase in each cell line was set as 1. The data represent a minimum of 394 kinetochores from five cells for each condition. P values were obtained using the Steel–Dwass multiple comparisons test. **(C)** Hec1-S55 phosphorylation during metaphase is dependent on Aurora A. Cells were treated with either DMSO or AZD1152 and/or MLN8237 for the last 1 h of the 3-h MG132 treatment, then fixed and stained with anti-Hec1 (green) and anti–phospho-Hec1-S55 (red) antibodies. DNA was stained with DAPI (blue). Boxed regions in the panels are shown as magnified images in insets. Scale bars: 5 µm (white), 500 nm (yellow). **(D)** Quantification of the Hec1-S55 phosphorylation signal in HeLa and RPE-1 cells during

metaphase. Relative intensity of the phospho-Hec1-S55 signal in cells treated as in C, which was calculated by dividing phospho-Hec1-S55 signal with Hec1 signal on each kinetochore, displayed as box and dot plots as in B. The median of DMSO-treated RPE-1 cells was set as 1. The data represent a minimum of 294 kinetochores from five cells for each condition. P values were obtained using the Steel multiple comparisons test. **(E)** Hec1-S55 phosphorylation in non-transformed and cancer cell lines during metaphase. Cells were treated with MG132 for 3 h and then fixed and stained with anti-Hec1 (green) and anti–phospho-Hec1-S55 (red) antibodies. DNA was stained with DAPI (blue). Boxed regions in the panels are shown as magnified images in insets. Scale bar: 5 µm (white), 500 nm (yellow). **(F)** Quantification of Hec1-S55 phosphorylation signal in nontransformed (blue), non-CIN (purple), and CIN (red) cancer cell lines during metaphase. Relative intensity of phospho-Hec1-S55 signal in cells treated as in E was calculated and displayed as box and dot plots as in B. The median of RPE-1 cells was set as 1. The data represent a minimum of 246 kinetochores from five cells for each cell line. P values were obtained using the Steel multiple comparisons test.

spindle, but not on spindle poles, was lost (Fig. 3 H). As shown in Fig. 3, I and J, Hec1-S55 phosphorylation was restored in mCherry-TPX2-WT–expressing cells, but not in mCherry-TPX2-3E–expressing cells, suggesting that Aurora A residing on the spindle is involved in the Hec1-S55 phosphorylation in metaphase.

To further confirm the result, we expressed the N-terminal fragment of TPX2 (TPX2-N; aa 1–43), which is sufficient for Aurora A binding and activation but lacks a microtubule binding domain (Bayliss et al., 2003). We found that mCherry–TPX2-N localized diffusely in the cytoplasm, and spindle localization of Aurora A was lost in mCherry–TPX2-N–expressing cells (Fig. 3 H). It is of note that the cytoplasmic Aurora A signal was increased in mCherry–TPX2-N–expressing cells (Fig. 3 H). In an immunoblot analysis, Aurora A expression was reduced when TPX2 was depleted, while it was increased in cells expressing mCherry-TPX2 constructs compared with parental cells (Fig. S4 B), probably reflecting the stabilization of Aurora A through binding to TPX2 (Giubettini et al., 2011), which implies that Aurora A was activated by binding to the TPX2 mutants. As shown in Fig. 3, I and J, Hec1-S55 phosphorylation was not restored in mCherry–TPX2-N–expressing cells, confirming the notion that Aurora A mislocalization from the spindle results in the less-efficient Hec1-S55 phosphorylation. We also examined the Hec1-S55 phosphorylation in cells expressing mCherry–Aurora A–S155R, a mutant unable to bind to TPX2 (Bibby et al., 2009), in RPE-1 cells containing Aurora A–mAID-mClover in the presence of IAA. mCherry–Aurora A–S155R localized to spindle poles but not to the spindle, whereas WT Aurora A or kinase-dead mutant Aurora A–K162R (Bischoff et al., 1998) fused with mCherry localized to both spindle poles and the spindle (Fig. S4 D). As shown in Fig. S4, D and E, mCherry–Aurora A restored the Hec1-S55 phosphorylation when Aurora A–mAID-mClover was depleted. In contrast, mCherry–Aurora A–S155R did not rescue the Hec1-S55 phosphorylation, similarly to mCherry–Aurora A–K162R (Fig. S4, D and E). Although mCherry–Aurora A–S155R cannot bind to TPX2 (Bibby et al., 2009), it was activated at spindle poles, which was confirmed by the autophosphorylation signal (Aurora A–pT288), in contrast to reduced autophosphorylation of Aurora A–K162R (Fig. S4, F and G), which is consistent with previous reports that Aurora A can be activated by autophosphorylation, which is different from activation by binding to TPX2 (Dodson and Bayliss, 2012; Zorba et al., 2014). These data suggest that Aurora A localizing to the spindle is mainly responsible for the Hec1-S55 phosphorylation during metaphase. It is noteworthy that Aurora A distribution on the spindle is more prominent in metaphase than in prometaphase (Fig. S4 H). This is probably due to increased microtubule mass in the metaphase spindle, owing to the formation of kinetochore fibers and their stabilization upon cyclin A destruction (Kabeche and Compton, 2013), which may underlie the Hec1-S55 phosphorylation on kinetochores at a distance from spindle poles.

Chromosome oscillation facilitates Aurora A–dependent phosphorylation of Hec1-S55 during metaphase

We addressed the relationship between chromosome oscillation and Hec1-S55 phosphorylation during metaphase, particularly whether chromosome oscillation promotes Hec1 phosphorylation. To test this, we altered the amplitude of chromosome oscillation by manipulating microtubule dynamics. First, we suppressed chromosome oscillation in RPE-1 cells by treating cells with a low dose of taxol, a microtubule stabilizer (Fig. 4, A and B; and Video 4). As shown in Fig. 4, C and D, Hec1-S55 phosphorylation was reduced by taxol treatment and was further reduced by inhibiting Aurora A. Next, we promoted chromosome oscillation in HeLa cells by depleting Kif18A, a kinesin-8 motor known to regulate chromosome oscillation (Stumpff et al., 2008; Fig. 4, E and F; Fig. S5 A; and Video 4). As shown in Fig. 4, G and H, the Hec1-S55 phosphorylation was increased by Kif18A depletion, and this was cancelled by inhibiting Aurora A. To corroborate these findings, we treated HeLa cells with BTB-1, a Kif18A inhibitor (Catarinella et al., 2009), which increased the amplitude of chromosome oscillation (Fig. S5, B and C; and Video 4) and confirmed that BTB-1 treatment increased Hec1-S55 phosphorylation during metaphase in an Aurora A–dependent manner (Fig. S5, D and E). In both Kif18A depletion and inhibition, Hec1-S55 phosphorylation was slightly reduced in the presence of AZD1152 (Fig. 4 H and Fig. S5 E), suggesting that Aurora B phosphorylates Hec1-S55 to some extent when Kif18A is suppressed, which may be caused by decreased interkinetochore distance (Mayr et al., 2007; Stumpff et al., 2008). We further addressed the relationship between chromosome oscillation and the Hec1-S55 phosphorylation by increasing microtubule dynamics in HeLa cells using UMK57, an agonist of the microtubule-destabilizing kinesin 13, MCAK (Orr et al., 2016). UMK57 treatment increased the amplitude of chromosome oscillation (Fig. 4, I and J; and Video 4), and in this condition, Hec1-S55 phosphorylation during metaphase was increased (Fig. 4, K and L). Collectively, these data suggest that chromosome oscillation facilitates Hec1-S55 phosphorylation during metaphase.

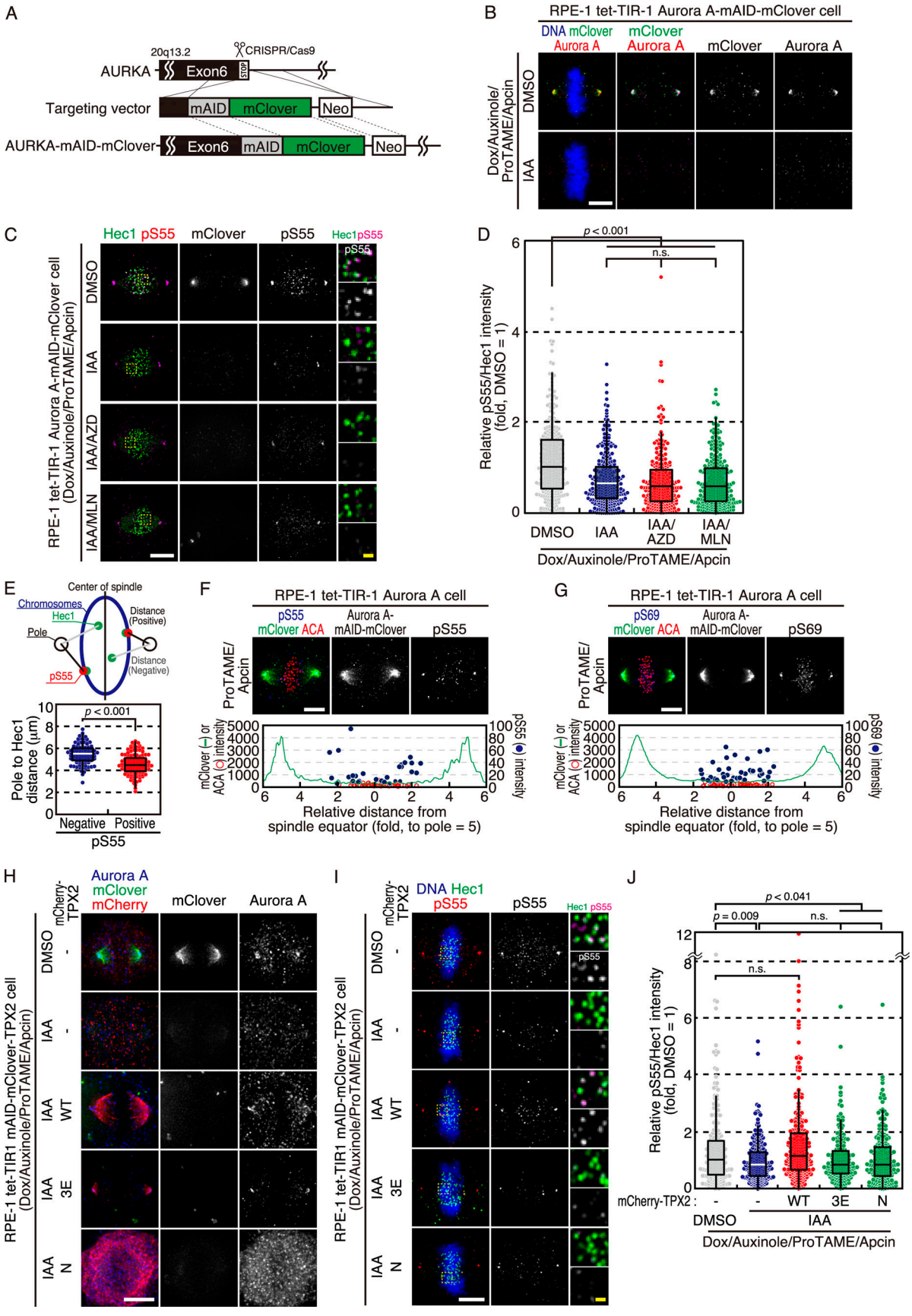

Figure 3. **Hec1-S55 phosphorylation during metaphase is mainly dependent on Aurora A localizing to the spindle. (A)** Schematic diagram of tagging endogenous Aurora A with mAID-mClover tag by the CRISPR/Cas–based method. **(B)** Depletion of Aurora A–mAID-mClover by adding IAA in RPE-1 cells

arrested in metaphase. Cells were treated as in Fig. S3 A with or without IAA, then fixed and stained with an anti–Aurora A (red) antibody. DNA was stained with DAPI (blue). The mClover signal (green) was acquired by fluorescence microscopy. Cells arrested in metaphase are shown. Scale bar: 5 µm. **(C)** Hec1-S55 phosphorylation in RPE-1 cells arrested in metaphase depleted of Aurora A using the AID system. Cells treated as in Fig. S3 A with or without AZD1152 and/or MLN8237 were fixed and stained with anti-Hec1 (blue, shown as green) and anti–phospho-Hec1-S55 (red) antibodies. The mClover signal (green, shown as monochrome) was acquired by fluorescence microscopy. Cells arrested in metaphase are shown. Boxed regions in the panels are shown as magnified images in insets. Scale bar: 5 µm (white), 500 nm (yellow). **(D)** Quantification of the Hec1-S55 phosphorylation signal in RPE-1 cells arrested in metaphase depleted of Aurora A using the AID system. Relative intensity of the phospho-Hec1-S55 signal in cells treated as in C was calculated and displayed as in Fig. 2 B. The median of DMSO-treated cells was set as 1. The data represent a minimum of 205 kinetochores from five cells for each condition. P values were obtained using the Steel–Dwass multiple comparisons test. **(E)** Quantification of distance between spindle pole and Hec1 signal on kinetochores depending on the Hec1-S55 phosphorylation. A schematic of measurement is shown at the top, and the result from 227 kinetochores from five cells is shown as box and dot plots as in Fig. 2 B. P value was obtained using the Mann–Whitney *U* test. **(F and G)** Phosphorylation of Hec1-S55 (F) or S69 (G) along the metaphase plate. Upper panels: Metaphase RPE-1 cells expressing Aurora A–mAID-mClover treated as in Fig. S3 A in the absence of IAA were fixed and stained with anti-GFP (green), anti–phospho-Hec1-S55 (F), or S69 (G; blue) and anti-centromere (ACA; red) antibodies. Scale bars: 5 µm. Lower graphs: Intensities of Aurora A–mAID-mClover (green), phospho-Hec1-S55 (F), or S69 (G; blue) and ACA (red) signals in the cells shown in the upper panels were plotted against relative distance from the spindle equator, where the distance from the spindle equator to a spindle pole was set as 5. **(H)** Replacement of endogenous TPX2 with WT TPX2 (WT), TPX2-F307E F334E F335E (3E), or the N-terminal fragment (aa 1–43) of TPX2 (N). RPE-1 cells containing mAID-mClover-TPX2 and expressing mCherry-TPX2 (WT, 3E, or N) were treated as in Fig. S3 A, then fixed and stained with anti-mCherry (red) or anti–Aurora A (blue). The mClover signal (green) was acquired by fluorescence microscopy. Cells arrested in metaphase are shown. Scale bar: 5 µm. **(I)** Hec1-S55 phosphorylation in RPE-1 cells arrested in metaphase expressing TPX2-WT, 3E, or N. Cells explained in H were treated as in Fig. S3 A, then fixed and stained with anti-Hec1 (green) and anti–phospho-Hec1-S55 (red) antibodies. DNA was stained with DAPI (blue). Cells arrested in metaphase are shown. Boxed regions in the panels are shown as magnified images in insets. Scale bar: 5 µm (white), 500 nm (yellow). **(J)** Quantification of the Hec1-S55 phosphorylation in RPE-1 cells arrested in metaphase expressing TPX2-WT, 3E, or N. Relative intensity of the phospho-Hec1-S55 signal in cells treated as in I was calculated and displayed as in Fig. 2 B. The median of DMSO-treated cells was set as 1. The data represent a minimum of 188 kinetochores from five cells for each condition. P values were obtained using the Steel–Dwass multiple comparisons test. AURKA, Aurora kinase A; Neo, neomycin resistance gene; Dox, doxycycline.

Aurora A–dependent Hec1 phosphorylation promotes chromosome oscillation

Chromosome oscillation was suppressed in metaphase-arrested RPE-1 cells treated with MLN8237, but not with AZD1152 (Fig. 5, A and B; and Video 5), confirming the recent finding that Aurora A, but not Aurora B, facilitates chromosome oscillation (DeLuca et al., 2018). We also confirmed the promotion of chromosome oscillation by Aurora A–dependent Hec1 phosphorylation by depleting Aurora A in Aurora A–mAID-mClover–expressing cells with IAA treatment (Fig. 5, C and D; and Video 5). We also found that the amplitude of chromosome oscillation was increased in HeLa cells treated with Calyculin A (Fig. S5, F and G; and Video 5), as expected. Overall, these data suggest that chromosome oscillation and Aurora A–dependent Hec1 phosphorylation promote each other.

Recently, it was reported that Hec1-S69 phosphorylation during metaphase promotes chromosome oscillation (DeLuca et al., 2018). Therefore, we explored the relationship between the phosphorylation of Hec1-S55 and -S69 on chromosome oscillation. When we treated HeLa cells with BTB-1 or UMK57, conditions that increase the amplitude of chromosome oscillation (Fig. 4, I and J; and Fig. S5, B and C), the level of Hec1-S69 phosphorylation was increased (Fig. S5, H and I); therefore, chromosome oscillation facilitates both Hec1-S69 and Hec1-S55 phosphorylation similarly. We further studied the dependency of chromosome oscillation on the phosphorylation of Hec1-S55 and -S69. We observed chromosome oscillation in metaphase-arrested RPE-1 cells expressing phosphorylation-site Hec1 mutants after depletion of endogenous Hec1. Chromosome oscillation amplitude was reduced in cells expressing Hec1-S55A (DeLuca et al., 2018; Fig. 5, E and F; Fig. S5 J; and Video 6). Cells expressing a Hec1 mutant in which S69 was mutated to alanine (Hec1-S69A) also showed reduction of chromosome oscillation (Fig. 5, E and F; Fig. S5 J; and Video 6). When both S55 and S69 were mutated (Hec1-2A), the amplitude of chromosome oscillation was even further reduced (Fig. 5, E and F; Fig. S5 J; and Video 6), suggesting that phosphorylation of both S55 and S69 of Hec1 is involved in chromosome oscillation. We also observed chromosome oscillation in cells expressing a Hec1 mutant in which all phosphorylation sites in the N-tail region except for S55 were mutated to alanine (eight out of nine sites; Hec1-8A55WT; DeLuca et al., 2018) and found that the amplitude of chromosome oscillation was reduced (Fig. 5 E and F; Fig. S5 J; and Video 6), showing that phosphorylation of Hec1-S55 alone cannot efficiently drive chromosome oscillation, confirming previous observations (DeLuca et al., 2018). Cells expressing a Hec1 mutant in which all the phosphorylation sites except S69 were mutated to alanine (Hec1-8A69WT) also showed a reduction of chromosome oscillation, but to a lesser extent (Fig. 5, E and F; Fig. S5 J; and Video 6). When both S55 and S69 were left unchanged while other phosphorylation sites were mutated (Hec1-7A2WT), chromosome oscillation was restored to the WT level (Fig. 5, E and F; Fig. S5 J; and Video 6). Taken together, phosphorylation of both Hec1-S55 and S69 by Aurora A promotes chromosome oscillation.

Chromosome oscillation promotes the correction of erroneous kinetochore–microtubule attachments during metaphase through Aurora A activity

CIN is a well-known property of cancer cells. Correction of erroneous kinetochore–microtubule attachments has been reported to occur not only in prometaphase but also in metaphase (Magidson et al., 2011). The findings that chromosome oscillation and metaphase Hec1-S55 phosphorylation were reduced in cancer cell lines prompted us to investigate whether they are also related to CIN. To address whether chromosome oscillation promotes the correction of erroneous kinetochore–microtubule attachments, we observed HeLa cells treated with BTB-1 or

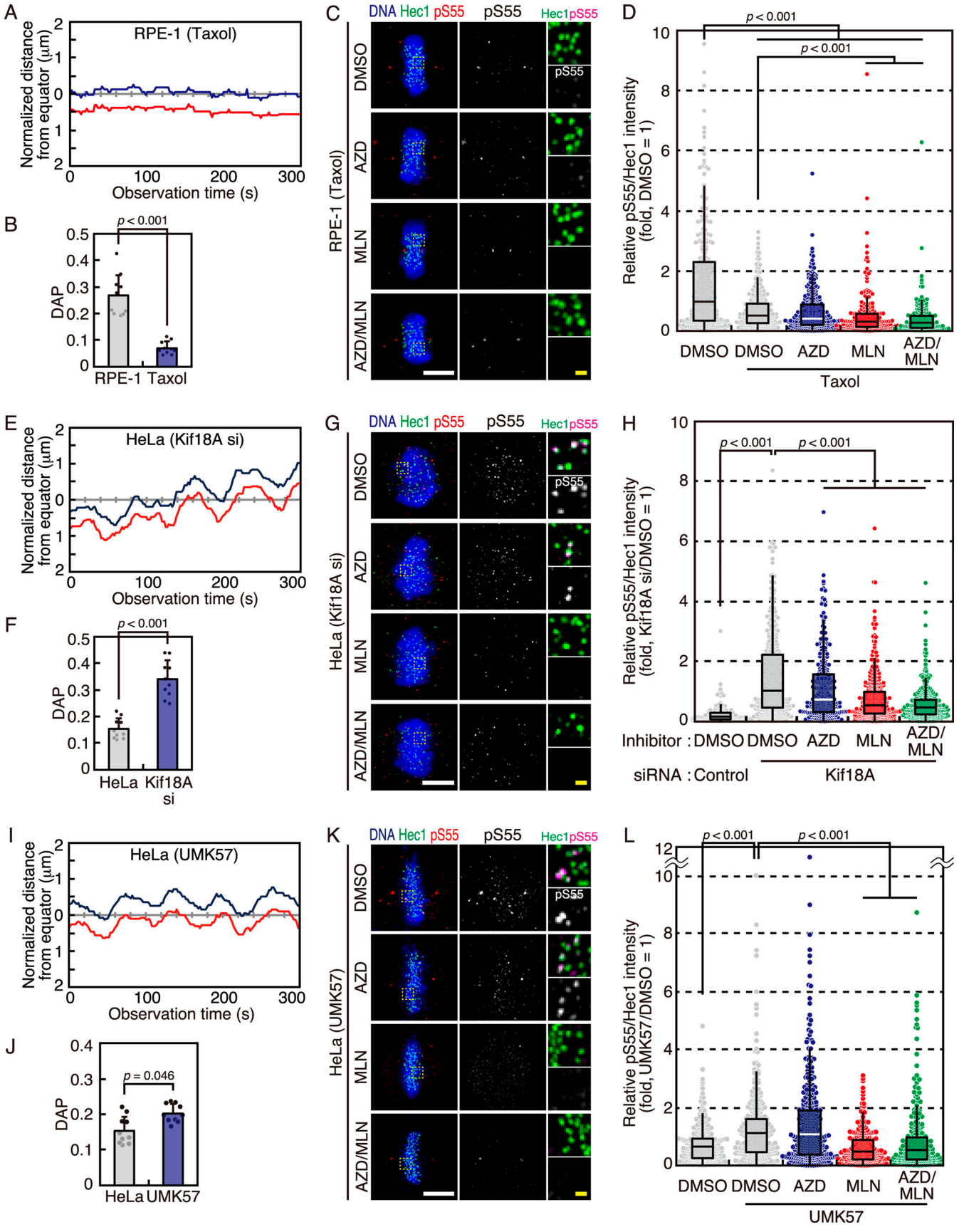

Figure 4. **Chromosome oscillation facilitates Aurora A–dependent phosphorylation of Hec1-S55 during metaphase. (A)** Trajectories of kinetochores in RPE-1 cells arrested in metaphase in the presence or absence of taxol. Cells were treated with or without 10 nM taxol for the last 1 h of a 2-h MG132 treatment

and observed by live-cell imaging. The blue and red trajectories show the movements of a pair of sister kinetochores in cells treated with taxol, plotted as the distance from the spindle equator. See also Video 4. **(B)** DAP measurements of kinetochore position in RPE-1 cells treated as in A. Error bars represent SD of 10 kinetochore pairs from three cells. P value was obtained using the Welch's *t* test. **(C)** Hec1-S55 phosphorylation in RPE-1 cells arrested in metaphase in the presence of taxol. Cells were treated with 10 nM taxol with either DMSO or AZD1152 and/or MLN8237 for the last 1 h of a 3-h MG132 treatment and then fixed and stained with anti-Hec1 (green) and anti–phospho-Hec1-S55 (red) antibodies. DNA was stained with DAPI (blue). Boxed regions in the panels are shown as magnified images in insets. Scale bar: 5 µm (white), 500 nm (yellow). **(D)** Quantification of the Hec1-S55 phosphorylation signal in RPE-1 cells treated as in C. Relative intensity of the phospho-Hec1-S55 signal was calculated and displayed as in Fig. 2 B. The median of DMSO-treated cells was set as 1. The data represent a minimum of 242 kinetochores from five cells for each condition. P values were obtained using the Steel multiple comparisons test. **(E)** Trajectories of kinetochores in HeLa cells arrested in metaphase with or without Kif18A depletion. Cells were treated with or without a Kif18A siRNA for 36 h, followed by 2-h MG132 treatment, and observed by live-cell imaging. The blue and red trajectories show the movements of a pair of sister kinetochores in cells depleted of Kif18A, plotted as the distance from the spindle equator. See also Video 4. **(F)** DAP measurements of kinetochore position in HeLa cells treated as in E. Error bars represent SD of 10 kinetochore pairs from three cells. P value was obtained using the Student's *t* test. **(G)** Hec1-S55 phosphorylation in HeLa cells arrested in metaphase depleted of Kif18A. Cells were treated with a Kif18A siRNA for 36 h, followed by treatment with either DMSO or AZD1152 and/or MLN8237 for the last 1 h during 3-h MG132 treatment, and then fixed and stained with anti-Hec1 (green) and anti–phospho-Hec1-S55 (red) antibodies. DNA was stained with DAPI (blue). Boxed regions in the panels are shown as magnified images in insets. Scale bar: 5 µm (white), 500 nm (yellow). **(H)** Quantification of the Hec1-S55 phosphorylation signal in HeLa cells treated as in G. Relative intensity of phospho-Hec1-S55 signal was calculated and displayed as in Fig. 2 B. The median of cells treated with the Kif18A siRNA and DMSO was set as 1. The data represent a minimum of 206 kinetochores from five cells for each condition. P values were obtained using the Steel multiple comparisons test. **(I)** Trajectories of kinetochores in HeLa cells arrested in metaphase in the presence or absence of UMK57, an MCAK potentiator. Cells were treated with or without UMK57 for the last 1 h of a 2-h MG132 treatment and observed by live-cell imaging. The blue and red trajectories show the movements of a pair of sister kinetochores in cells treated with UMK57, plotted as the distance from the spindle equator. See also Video 4. **(J)** DAP measurements of kinetochore position in HeLa cells treated as in I. Error bars represent SD of 10 kinetochore pairs from three cells. P value was obtained using the Student's *t* test. **(K)** Hec1-S55 phosphorylation in HeLa cells during metaphase in the presence of UMK57. Cells were treated with UMK57 and either DMSO or AZD1152 and/or MLN8237 for the last 1 h of a 3-h MG132 treatment, then fixed and stained with anti-Hec1 (green) and anti–phospho-Hec1-S55 (red) antibodies. DNA was stained with DAPI (blue). Cells arrested in metaphase are shown. Boxed regions in the panels are shown as magnified images in insets. Scale bar: 5 µm (white), 500 nm (yellow). **(L)** Quantification of the Hec1-S55 phosphorylation signal in HeLa cells treated as in K. Relative intensity of phospho-Hec1-S55 signal was calculated and displayed as box and dot plots as in Fig. 2 B. The median of UMK57-treated cells without Aurora inhibitors was set as 1. The data represent a minimum of 213 kinetochores from five cells for each condition. P values were obtained using the Steel multiple comparisons test. Kif18Asi, treatment with an siRNA for Kif18A.

UMK57, treatments that promote chromosome oscillation (Fig. 4, I and J; and Fig. S5, B and C). We examined the incidence of lagging chromosomes in anaphase/telophase cells released from metaphase arrest and found that it was reduced in cells treated with BTB-1 or UMK57 (Fig. 6, A and B). We also examined the incidence of merotelic attachments by observing kinetochore–microtubule attachment in metaphase-arrested cells and found that this also was reduced in cells treated with BTB-1 or UMK57 (Fig. S5, K and L). These data suggest that chromosome oscillation promotes the correction of erroneous kinetochore–microtubule attachments.

Next, we addressed the role of Aurora A in error correction during metaphase. We found that the incidence of cells with lagging chromosomes as well as merotelic attachments was increased by inhibiting Aurora A (Fig. 6 C and Fig. S5 M), suggesting that Aurora A is involved in error correction, in line with previous reports (DeLuca et al., 2018; Ye et al., 2015). We confirmed these results by depleting Aurora A in the Aurora A–mAID-mClover–expressing cells with IAA treatment and found that the number of cells with lagging chromosomes was increased (Fig. 6 C). Increased numbers of cells with lagging chromosomes and merotelic attachments were also seen when Aurora B was inhibited, probably due to the effect on cells that entered mitosis after release from the MG132 treatment (Fig. 6 C and Fig. S5 M). We confirmed that the spindle structure was maintained when Aurora A and/or B was inhibited in metaphase-arrested cells at the concentration used in the experiment (Fig. S5, N and O), excluding the possibility that the increase in the cells with lagging chromosomes and merotelic attachments is due to disruption of the spindle structure. These data suggest that Aurora A promotes the correction of erroneous kinetochore–microtubule attachments during metaphase.

We also studied the contribution of phosphorylation of Hec1-S55 and -S69 to error correction. The number of cells with lagging chromosomes was increased in cells depleted of endogenous Hec1 expressing Hec1-S69A (Fig. 6 D). In cells expressing Hec1-S55A, there was no significant increase in cells with lagging chromosomes, but Hec1-2A–expressing cells exhibited a marked increase of cells containing lagging chromosomes compared with Hec1-S69A–expressing cells (Fig. 6 D). Although the effects shown here are not confined to metaphase in this experimental setting, these data suggest that Hec1-S55 phosphorylation contributes cooperatively with Hec1-S69 phosphorylation to error correction.

Discussion

We found that chromosome oscillation is attenuated in cancer cell lines, and this is correlated with reduced Hec1-S55 phosphorylation during metaphase. The Hec1-S55 phosphorylation during metaphase was mainly dependent on Aurora A residing at the spindle, but not on Aurora B. Chromosome oscillation and phosphorylation of Hec1-S55 as well as Hec1-S69 by Aurora A during metaphase promote each other and play a role in the correction of erroneous kinetochore–microtubule attachments. Physiological roles for chromosome oscillation have been proposed, such as prevention of entanglement or damage of chromosomes (Ke et al., 2009). The correction of erroneous kinetochore–microtubule attachments may be another, previously unrecognized, role of chromosome oscillation. Our data imply that attenuated chromosome oscillation, related to

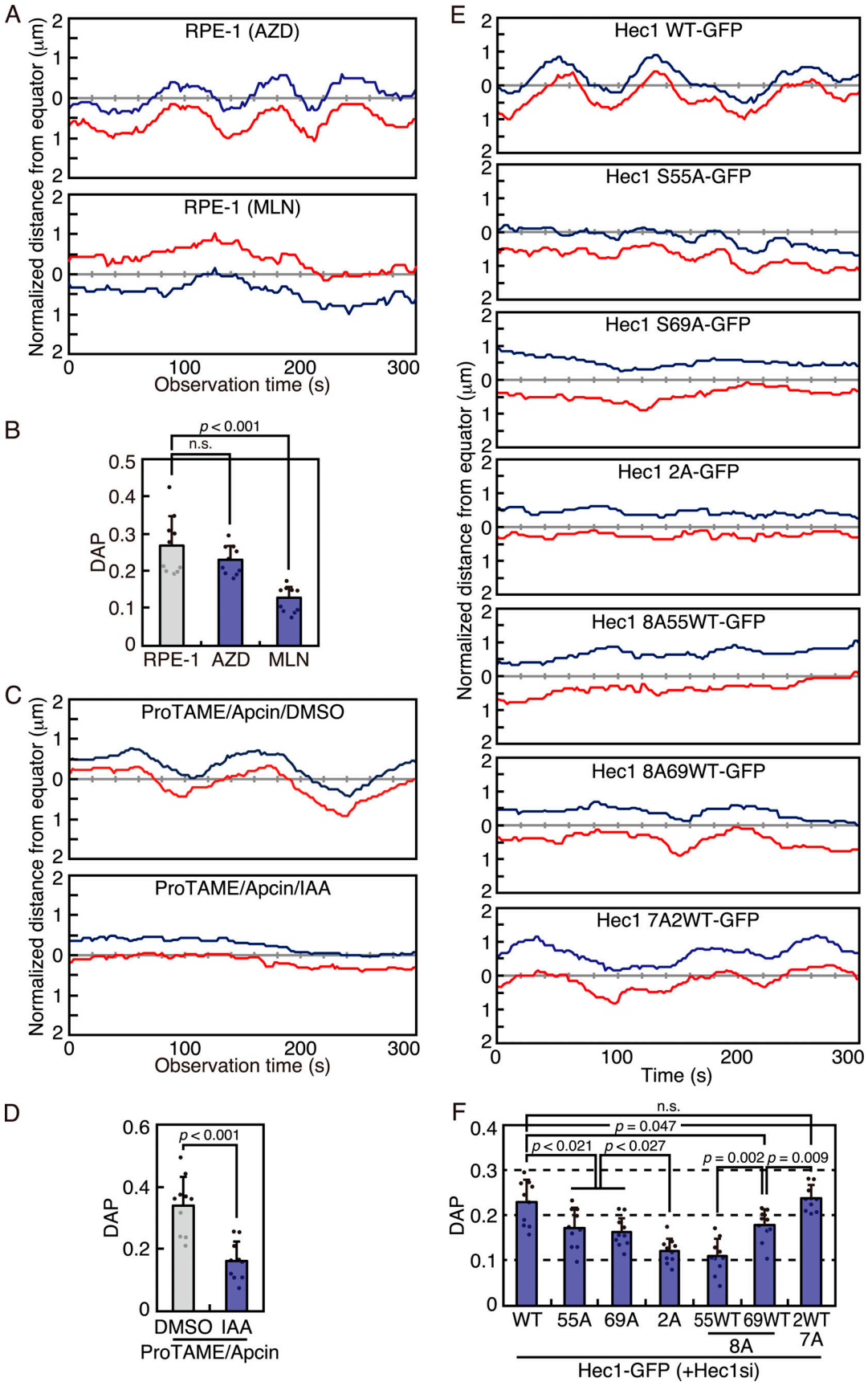

Figure 5. **Aurora A–dependent Hec1 phosphorylation promotes chromosome oscillation. (A)** Trajectories of kinetochores in RPE-1 cells arrested in metaphase in the presence or absence of Aurora inhibitors. Cells were treated with AZD1152 or MLN8237 for the last 1 h of a 2-h MG132 treatment and

observed by live-cell imaging. The blue and red trajectories show the movements of a pair of sister kinetochores in cells treated with AZD1152 (upper) or MLN8237 (lower), plotted as the distance from the spindle equator. See also Video 5. **(B)** DAP measurements of kinetochore position in RPE-1 cells treated as in A. Error bars represent SD of 10 kinetochore pairs from three cells. P values were obtained using the Dunnett's multiple comparisons test. **(C)** Trajectories of kinetochores in RPE-1 cells arrested in metaphase depleted of Aurora A by the AID system. RPE-1 cells containing Aurora A–mAID-mClover were treated as in Fig. S3 A with or without IAA and observed by live-cell imaging. The blue and red trajectories show the movements of a pair of sister kinetochores in nontreated cells (upper) or IAA-treated cells (lower), plotted as the distance from the spindle equator. See also Video 5. **(D)** DAP measurements of kinetochore position in RPE-1 cells treated as in C. Error bars represent SD of 10 kinetochore pairs from three cells. P value was obtained using the Student's *t* test. **(E)** Trajectories of kinetochores in RPE-1 cells arrested in metaphase depleted of endogenous Hec1 and expressing EGFP-tagged WT Hec1 or Hec1 mutants, in which phosphorylation sites are mutated to alanine. Cells expressing Hec1-WT, Hec1-S55A, or S69A, a single phosphorylation site mutant; Hec1-2A, in which both S55 and S69 are mutated to alanine; or Hec1 mutants in which all phosphorylation sites are mutated to alanine except for S55 (8A55WT), S69 (8A69WT), or both (7A2WT) were arrested in metaphase by 2-h MG132 treatment and observed by live-cell imaging. The blue and red trajectories show the movements of a pair of sister kinetochores in cells expressing each Hec1 construct, plotted as the distance from the spindle equator. See also Video 6. **(F)** DAP measurements of kinetochore position in RPE-1 cells treated as in E. Error bars represent SD of 10 kinetochore pairs from three cells. P values were obtained using the Tukey–Kramer multiple comparison test.

reduced Hec1-S55 phosphorylation by Aurora A during metaphase, is a cause of CIN in cancer cell lines.

It is well known that Aurora B, which mainly localizes to inner centromeres, contributes to the correction of erroneous kinetochore–microtubule attachments by phosphorylating Hec1 during prometaphase (Cimini et al., 2006; DeLuca et al., 2006; Lampson and Cheeseman, 2011; Fig. 6 E). Aurora A also destabilizes erroneous attachments by phosphorylating Hec1 when kinetochores are near spindle poles (Chmátal et al., 2015; Ye et al., 2015). In metaphase, when kinetochores are under tension and become distant from inner centromeres, Aurora B activity on kinetochores is reduced (Lampson and Cheeseman, 2011), which is further facilitated by reduced inner centromere localization of Aurora B (Salimian et al., 2011) and increased phosphatase activity (Asai et al., 2019; Saurin, 2018). Our data suggest that the phosphorylation of Hec1-S55 and -S69 by Aurora A during metaphase is a mechanism to eliminate the remaining erroneous attachments to ensure bi-orientation establishment for all the chromosomes (Fig. 6 E). Our findings that (1) Aurora A residing on the spindle, rather than at the spindle poles, was mainly responsible for the Hec1-S55 phosphorylation (Fig. 3, I and J; and Fig. S4, D and E); (2) Hec1-S55 is preferentially phosphorylated on kinetochores at the edge of the metaphase plate (Fig. 3, E and F); and (3) there is a declining Aurora A gradient along the spindle axis from poles to the equator (Fig. 3, F and G) suggest poleward chromosome motion during oscillation increases the chance of Hec1-S55 phosphorylation on kinetochores by Aurora A as they move transiently closer to spindle poles (Fig. 6 E). This is similar to the mechanism by which Aurora A acts on chromosomes near the spindle poles during prometaphase in mitosis and meiosis (Chmátal et al., 2015; Ye et al., 2015). However, we assume that this Aurora A "gradient" is not just a density gradient of a soluble pool of Aurora A turning over on spindle poles, but rather a gradient of spindle-associated Aurora A formed by dynein-dependent transport of TPX2 (Ma et al., 2010) due to the following reasons: (1) Aurora A localization gradient is only seen on the spindle, but not at all directions around spindle poles (Fig. 3 F) and (2) Aurora A localization on the spindle becomes apparent in metaphase when mature K-fibers are formed (Fig. S4 H). Aurora A activated and recruited to microtubules near spindle poles by TPX2 was reported to play a role in removing contractility components from the polar cortex in *Caenorhabditis elegans* (Mangal et al., 2018). The increased Aurora A distribution on the spindle during metaphase may extend the phosphorylation gradient closer to the metaphase plate. Hec1 phosphorylation is considered to promote error correction by increasing microtubule turnover at kinetochores (Wimbish and DeLuca, 2020). Recently, it was reported that Hec1 phosphorylation specifically affects kinetochore coupling to polymerizing microtubules (Long et al., 2017). As a leading kinetochore is closer to a spindle pole than a trailing kinetochore is, Hec1 on the leading kinetochore would be preferentially phosphorylated at the edge of the metaphase plate. Therefore, one possibility is that merotelic attachments on the leading kinetochores are preferentially destabilized because merotelically attached microtubules are in a polymerizing state at the edge of the metaphase plate. Even if both merotelically and correctly attached microtubules are destabilized, fewer numbers of merotelically attached microtubules against correctly attached microtubules and higher density of microtubules from closer spindle poles for leading kinetochores may facilitate error correction. The Hec1-S69 phosphorylation, which was reported to be dependent on a fraction of Aurora A at the inner centromere (DeLuca et al., 2018), occurs throughout the metaphase plate (Fig. 3 G), but the observed increase in Hec1-S69 phosphorylation level in HeLa cells upon facilitating chromosome oscillation (Fig. S5, H and I) implies that it can also be phosphorylated by Aurora A on the spindle. How different phosphorylation sites on the Hec1 N-tail are phosphorylated by Aurora kinases in different circumstances is currently unknown. The local environment around the phosphorylation sites, such as the influence of phosphatases as previously proposed (DeLuca et al., 2018), may be different at individual phosphorylation sites. Aurora A and B share many of their substrates (Hochegger et al., 2013), and they mainly suppress (by phosphorylating Hec1 [Cimini et al., 2006; Lampson and Cheeseman, 2011], CENP-E [Kim et al., 2010], and the Ska complex [Schmidt et al., 2012], etc.), but sometimes promote (by phosphorylating HURP [Koffa et al., 2006; Wong and Fang, 2006], etc.) the formation of stable kinetochore–microtubule attachments. Whether other substrates are regulated through oscillation-dependent phosphorylation by Aurora A requires further study.

While chromosome oscillation facilitates Hec1 phosphorylation, Aurora A–dependent Hec1 phosphorylation at both S55 and S69 promotes chromosome oscillation (Fig. 5, E and F). Among

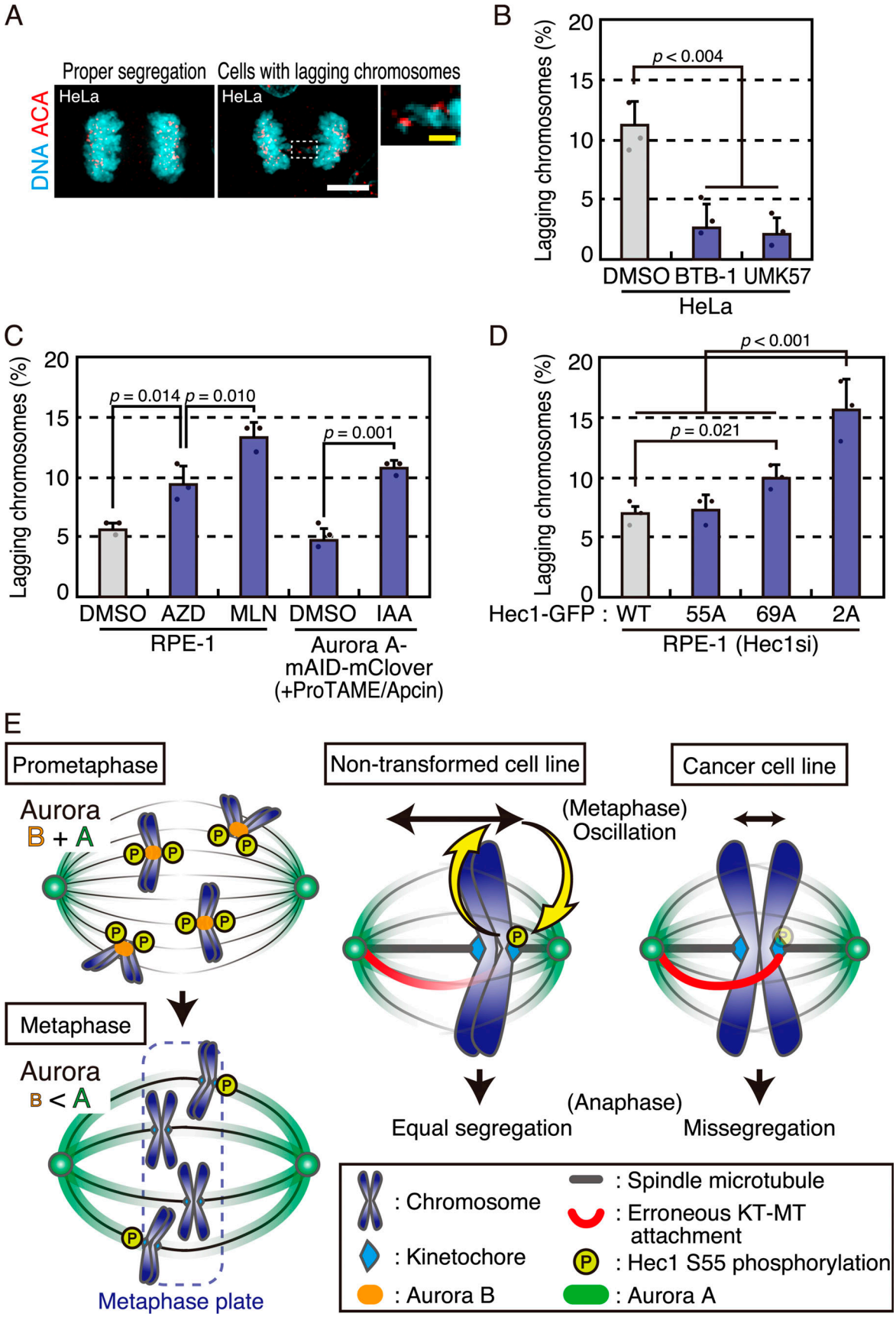

Figure 6. **Chromosome oscillation promotes the correction of erroneous kinetochore–microtubule attachments during metaphase through Aurora A activity. (A)** Lagging chromosomes in HeLa cells. Cells were treated with either DMSO, BTB-1, or UMK57 for the last 1 h of a 3-h MG132 treatment, then

released from the drug treatment for 1.5 h, fixed, and stained with anti-centromere antibodies (ACAs) and DAPI. Anaphase/telophase cells were examined for the presence or absence of lagging chromosomes (inset). Scale bar: 5 µm (white), 500 nm (yellow). **(B)** Quantification of HeLa cells containing lagging chromosomes in the presence of BTB-1 or UMK57. Cells were treated, fixed, and stained as in A. Frequency of anaphase/telophase cells containing lagging chromosomes was quantified. Error bars represent SD of three independent experiments, in which a minimum of 100 cells were observed for each condition. P values were obtained using the Dunnett's multiple comparisons test. **(C)** Quantification of RPE-1 cells containing lagging chromosomes in the presence of AZD1152 or MLN8237 or depleted of Aurora A by the AID system. Cells were treated with either DMSO, AZD1152, or MLN8237 for the last 1 h of a 3-h MG132 treatment, then released from the drug treatment for 1.5 h before fixation. For RPE-1 cells containing Aurora A–mAID-mClover, they were treated with doxycycline and auxinole for 24 h and treated with or without IAA for the last 1 h of a 3-h proTAME and apcin treatment, then released from the drug treatment for 1.5 h before fixation. Cells were stained as in A, and frequency of anaphase/telophase cells containing lagging chromosomes was quantified. Error bars represent SD of three independent experiments, in which a minimum of 100 cells were observed for each condition. P values were obtained using the Dunnett's multiple comparisons test. **(D)** Quantification of RPE-1 cells containing lagging chromosomes depleted of endogenous Hec1 expressing Hec1-WT-GFP, Hec1-S55A-GFP, Hec1-S69A-GFP, or Hec1-2A-GFP shown in Fig. 5 E. Cells were stained as in A, and frequency of anaphase/telophase cells containing lagging chromosomes was quantified. Error bars represent SD of three independent experiments, in which a minimum of 100 cells were observed for each condition. P values were obtained using the Tukey–Kramer multiple comparisons test. **(E)** Model of correction of erroneous kinetochore (KT)–microtubule (MT) attachments by Aurora kinases. Left panels: During prometaphase, Hec1 on kinetochores is phosphorylated by Aurora B (orange), which resides at the inner centromere, as well as by Aurora A (green), which localizes mainly to spindle poles, thus facilitating correction of erroneous kinetochore–microtubule attachments. In metaphase, Hec1 phosphorylation by Aurora B is reduced, while the Aurora A that localizes to the spindle phosphorylates Hec1-S55 when kinetochores approach close to spindle poles during chromosome oscillation, thus contributing to elimination of any remaining erroneous kinetochore–microtubule attachments. Right panels: In nontransformed cell lines, chromosome oscillation facilitates the Hec1-S55 phosphorylation by Aurora A, and this in turn increases the amplitude of chromosome oscillation together with the Hec1-S69 phosphorylation, thereby promoting the correction of erroneous kinetochore–microtubule attachments (red). In cancer cell lines, chromosome oscillation is attenuated, which leads to reduced Hec1-S55 phosphorylation by Aurora A, resulting in inefficient correction of erroneous attachments and increase in chromosome missegregation.

the nine phosphorylation sites on the Hec1 N-tail, it was estimated that only a couple of sites are phosphorylated during metaphase, and these are sufficient for chromosome oscillation (Zaytsev et al., 2014). Therefore, phosphorylation of Hec1-S55 and -S69 may be good enough to support chromosome oscillation during metaphase. Our data suggest that there is positive feedback between chromosome oscillation and Hec1 phosphorylation by Aurora A, ensuring elimination of erroneous kinetochore–microtubule attachments (Fig. 6 E). However, as Hec1-S69 phosphorylation, which is seen in every cell line tested irrespective of oscillation amplitude, can support a certain level of chromosome oscillation in RPE-1 cells (Fig. 5, E and F), oscillation amplitude in each cell line may be determined independently of Aurora A activity. Rather, Hec1 phosphorylation at S55 and S69 by Aurora A may allow the inherent level of chromosome oscillation by increasing turnover of K-fibers. Therefore, we assume that robust chromosome oscillation is the intrinsic property of nontransformed cell lines, and resulting Hec1-S55 phosphorylation may reinforce chromosome oscillation. In addition to Hec1 phosphorylation, chromosome oscillation may also promote error correction by facilitating MCAK activity through suppression of α-tubulin de-tyrosination, as was recently reported (Ferreira et al., 2020). In physiological conditions, chromosome oscillation declines as cells progress toward anaphase (Häfner et al., 2014), which may represent the final stabilization of kinetochore–microtubule attachments before chromosome segregation.

We found that chromosome oscillation is reduced in cancer cell lines (Fig. 1). When we quantified the expression of Aurora A and TPX2 on the spindle by immunofluorescence (IF) staining in the cell lines used in this study, we found no general trend distinguishing cancer cell lines from nontransformed cell lines that might explain reduced chromosome oscillation in cancer cell lines (Fig. S5 P). Chromosome oscillation is regulated by the activity of motor proteins and microtubule dynamics (Jaqaman et al., 2010; Stumpff et al., 2008; Stumpff et al., 2012). It was reported that microtubule stability is increased in cancer cell lines (Bakhoum et al., 2009a; Bakhoum et al., 2009b), which may be a cause of reduced chromosome oscillation in these cells. Two kinesin 13 motor proteins, Kif2b and MCAK, stimulate kinetochore–microtubule dynamics during prometaphase and metaphase, respectively, and depletion of either protein increases chromosome missegregation (Bakhoum et al., 2009b), implying that proper microtubule dynamics is essential for mitotic fidelity not only in prometaphase but also in metaphase (Bakhoum and Compton, 2012b). We show that the amplitude of chromosome oscillation is increased in HeLa cells by MCAK activation (Fig. 4, I and J), supporting the possibility that increased microtubule stability is a cause of attenuated chromosome oscillation in cancer cell lines. Although we found that increased chromosome oscillation by Kif18A inhibition in HeLa cells reduced the rate of chromosome missegregation (Fig. 6 B), it was recently reported that Kif18A depletion in RPE-1 cells results in increased micronuclei formation due to scattering of chromosomes during anaphase, in spite of the absence of chromosome missegregation (Fonseca et al., 2019), suggesting that the amplitude of chromosome oscillation should be regulated within a proper range. Whether the attenuated chromosome oscillation is a property of cancer cells in vivo is an important issue to be addressed. Interestingly, we found that "non-CIN" cancer cell lines exhibit an intermediate level of chromosome oscillation as well as Hec1-S55 phosphorylation between nontransformed cell lines and CIN cancer cell lines (Fig. 1 D and Fig. 2 F). We also found that these cell lines actually have low levels of CIN (Fig. S1, C and D), further implying the correlation between the level of chromosome oscillation and the level of CIN.

In conclusion, our study has uncovered another layer in the mechanism for correction of erroneous kinetochore–microtubule attachments that ensures faithful chromosome segregation, and one that is defective in cancer cell lines. Even if the majority of erroneous attachments are corrected during

prometaphase, mainly by Aurora B (Cimini et al., 2006; Hauf et al., 2003), persistence into metaphase of a small number of uncorrected erroneous attachments may cause CIN in cancer cell lines. In terms of cancer therapy, accelerating CIN above the tolerable threshold is proposed as a strategy to kill cancer cells (Tanaka and Hirota, 2016). Suppressing chromosome oscillation can thus be used for cancer therapy, and this may be one of the mechanisms of action of taxol, a drug that suppresses microtubule dynamics (Yvon et al., 1999). Further studies are required to elucidate the role of chromosome oscillation in mitotic fidelity and the relationship between reduced chromosome oscillation and CIN in cancer cells.

Materials and methods

Plasmids and antibodies

Monoclonal mouse antibodies were used as follows: anti-Hec1 9G3 (Abcam; ab3613) for Western blotting (WB) 1:2,000, for IF 1:1,000; anti-α-tubulin B-5-1-2 (Merck; T5168) WB 1:5,000, IF 1:3,000; anti–AIM-1 clone 6/AIM-1 (anti–Aurora B; BD Bioscience; 611082) WB 1:2,000, IF 1:1,000; Living Colors mCherry Monoclonal Antibody (Takara Bio; 632543) WB 1:3,000, IF 1:2,000; anti-TPX2 18D5-1 (Novus Biologicals; NB100-74556) WB 1:2,000, IF 1:1,000; and anti-GFP clones 7.1 and 13.1 (Merck; 11814460001) IF 1:1,000. A monoclonal rabbit antibody was used as follows: anti-phospho–Aurora A Thr288 C39D8 (Cell Signaling Technology; 3079S) IF 1:1,000. Polyclonal rabbit antibodies were used as follows: anti–phospho-Hec1 Ser 55 (GeneTex; GTX70017) IF 1:1,000; anti-Pericentrin (Abcam; ab4448) IF 1:1,000; anti–Aurora A (Abcam; ab12875) WB 1:2,000, IF 1:1,000; anti-INCENP (P240; Cell Signaling Technology; #2807) WB 1:500; anti-Kif18A (Bethyl Laboratories; A301-080A) WB 1:2,000; anti-GFP (Life Technologies; A11122) IF 1:2,000; and anti–α-tubulin (Abcam; ab18251) IF 1:1,000. Anti-centromere protein human autoimmune serum (Antibodies Inc.; 15–234) was used for IF 1:3,000. We also used anti–phospho-Hec1 Ser 69 (gift from J.G. DeLuca; IF 1:1,000; DeLuca et al., 2011; DeLuca et al., 2018). The blocking peptide for the Hec1-S55 phosphorylation was purchased from GeneTex. The Aurora A cDNA fragment was amplified from the MegaMan Human Transcriptome cDNA library (Agilent Technologies) using the following primers: 5′-AGCTGGTACCATGGACCGATCTAAA-3′ and 5′-CAGTGGATCCCTAAGACTGTTTGCT-3′ (J-Bios). The TPX2 (aa 1–43) cDNA fragment was amplified from the pmCherry-TPX2 using the following primers: 5′-GCTTCAAGGTGCACATGGAG-3′ and 5′-GAAGGCCAATTTGGAGAATGGATCCATGC-3′ (J-Bios). These cDNAs were subcloned into Kpn I/BamH I and Sal I/BamH I sites of the pmCherry-C1 vector (Takara Bio), respectively. For construction of targeting vector for the mAID-mClover tagging of Aurora A and B, a 446-bp homology arm containing a BamH I site in place of a stop codon was subcloned into EcoR V site of the pUC57 by Genewiz. The mAID-mClover cDNA fragment including a marker gene, taken from pMK289 (Addgene plasmid #72827), was then subcloned into the BamH I site (Natsume et al., 2016). For construction of targeting vector for the mAID-mClover tagging of TPX2, a 1,000-bp homology arm, which was amplified from the genomic DNA of RPE-1 cell using primers 5′-ATGCGAGCTCTGCTGATTACT TAAAGATAA-3′ and 5′-ATGCGGTACCGCTGCCATCACTAC AGACAT-3′ (J-Bios), was subcloned into Sac I/Kpn I sites of the pBluescript II KS(−) (Agilent Technologies), and start codon was exchanged with Sal I/BamH I sites by inverse PCR using the following primers: 5′-ATGCGGATCCATGTCACAAGTTAAAAG CTC-3′ and 5′-ATGCGTCGACTGTCTCCCACTTAACGCAGAAGA GCACG-3′ (J-Bios). The mAID-mClover cDNA fragment including a marker gene, taken from pMK348 (Addgene plasmid #121182), was subcloned into the Sal I/BamH I sites (Yesbolatova et al., 2019). The single-guide RNAs (sgRNAs) for the CRISPR/Cas9 system were subcloned into pX330-U6-Chimeric_BB-CBh-hSpCas9, which was a gift from Feng Zhang (Broad Institute, Inc., Cambridge, MA; Addgene plasmid #42230; Cong et al., 2013). The pmCherry-TPX2 was a gift from Patricia Wadsworth (University of Massachusetts, Hadley, MA; Addgene plasmid #31227; Ma et al., 2010). The plasmid DNAs containing Hec1-GFP WT, 8A55WT, and 8A69WT were gifted from J.G. DeLuca (Colorado State University, Fort Collins, CO; DeLuca et al., 2018; Guimaraes et al., 2008). The plasmid DNAs containing mCherry–Aurora A S155R, K162R, mCherry-TPX2 F307E/F334E/H335E, Hec1-GFP-55A, 69A, 2A, and 7A2WT were made using the Quick-Change method (Agilent Technologies).

RNA interference

An RNA oligonucleotide targeting 5′ UTR for Hec1 was 5′-CCC UGGGUCGUGUCAGGAATT-3′ (DeLuca et al., 2011; J-Bios). Targeted sequences for INCENP and Kif18A were 5′-CAGUGUAGA GAAGCUGGCUACAGUG-3′ (Abe et al., 2016) and 5′-GAACAG AUUCGUGAUCUCUUAGUAA-3′ (Stealth; Thermo Fisher Scientific), respectively. For control siRNA, Stealth RNAi siRNA negative control med GC duplex #2 was used (Thermo Fisher Scientific). RNA duplexes (50 nM) were transfected into cells using Lipofectamine RNAiMAX reagent (Thermo Fisher Scientific).

Cell culture and synchronization

RPE-1 cells (a gift from H. Hochegger; University of Sussex, Brighton, UK), HCT116 cells (human colorectal carcinoma cells, CCL-247; American Type Culture Collection [ATCC]), HeLa Kyoto cells (human cervical carcinoma cells; a gift from T. Hirota; The Cancer Institute of Japanese Foundation for Cancer Research, Ariake, Tokyo, Japan), DU145 cells (human prostate carcinoma cells, HTB-81; ATCC), A549 cells (human lung adenocarcinoma cells, CCL-185; ATCC), U2OS cells (human osteosarcoma cells; gift from T. Hirota), and MCF-7 cells (human breast adenocarcinoma cells, HTB-22; ATCC) were grown at 37°C in a 5% CO_2 atmosphere in DMEM (Nacalai), supplemented with 10% fetal bovine serum. HCT-15 cells and DLD-1 cells (human colorectal carcinoma cells, TKG 0504 and TKG 0379; Cell Resource Center for Biomedical Research, Institute of Development, Aging and Cancer, Tohoku University, Sendai, Miyagi, Japan) were grown in RPMI1640 (Nacalai) supplemented with 10% fetal bovine serum. Normal human diploid lung fibroblasts (TIG-3 cells; Health Science Research Resources Bank) were grown in DMEM high-glucose GlutaMAX (Thermo Fisher Scientific), supplemented with 10% fetal bovine serum. Cells were synchronized by 20 µM MG132 (Merck) for 3 h for IF analysis

and for 2 h for live-cell imaging. For WB, cells were synchronized by 1 µM Eg-5 inhibitor III (Merck) for 18 h and were treated with 20 µM MG132 for 3 h after washing out Eg5 inhibitor III. Cells were treated for 1 h before analysis with indicated inhibitors (100 nM AZD1152 [Merck], 50 nM MLN8237 [Cayman Chemical], 50 nM BTB-1 [Tocris Bioscience], 100 nM UMK57 [AOBIOUS], 10 nM taxol [Merck], and 10 nM Calyculin A [Cell Signaling]).

For RNAi experiments, cells were transfected with siRNAs for 36 h and then used for further experiments. For the generation of Aurora A– and Aurora B–mAID-mClover and mAID-mClover-TPX2–expressing cells, tet-OsTIR-1-puro was inserted to the AAV1 locus in RPE-1 cells using the CRISPR/Cas9 system, and positive cells were cloned using puromycin (Hayashi et al., 2012; Natsume et al., 2016). The targeted sgRNA sequences for Aurora A, Aurora B, and TPX2 were 5′-GTCAGGTTATATGGC AGCCCTGG-3′, 5′-CCCTTCAATCTGTCGCCTGATGG-3′, and 5′-GCTCTTCTGCGTTAAGTGGGTGG-3′ (J-Bios), respectively. sgRNA-hSpCas9 plasmids and the targeting vectors were transfected using the Neon Transfection System (Thermo Fisher Scientific), and stable transformants were selected with 1 mg/ml G418 (Nacalai) for tagging Aurora A/B or 5 µg/ml Blasticidin S (Wakenyaku Co., Ltd.) for tagging TPX2. Before experiments, the mAID-mClover–tagged cells were treated with 1 µg/ml doxycycline (Merck), 200 µM auxinole (Hayashi et al., 2012), 20 µM ProTAME (Boston Biochem), and 50 µM apcin (Cayman Chemical) according to the procedure shown in Fig. S3 A. The cells were treated with 500 µM IAA (Merck) for 1 h and used for further analysis. In rescue experiments using Aurora A constructs, plasmids were transfected into cells with FuGENE HD (Promega) for 24 h before siRNA transfection or doxycycline treatment. In rescue experiments using TPX2 constructs, plasmids were transfected into cells with FuGENE HD (Promega), and stable transformants were selected by treatment with 1 mg/ml G418 for 2 wk.

IF analysis

Cells were grown on a glass coverslip and fixed with methanol at −20°C for 5 min. In Fig. 2 A; Fig. 3, B, C, and H; Fig. S2, I and K; Fig. S3, D, E, and H; Fig. S4, C, D, F, and H; and Fig. S5, H, N, and P, cells were fixed with 3% paraformaldehyde in PBS (137 mM NaCl, 2.7 mM KCl, 10 mM Na_2HPO_4, and 1.8 mM KH_2PO_4, pH 7.4) for 10 min at 37°C and permeabilized with 1% Triton X-100 in PBS for 5 min. In Fig. S5 K, cells were fixed with 1% glutaraldehyde in PHEM buffer (60 mM Pipes, 25 mM Hepes, 10 mM EGTA, and 2 mM $MgCl_2$) for 10 min at 37°C and quenched with 0.1 g/ml $NaBH_4$ in PHEM buffer for 10 min. Before fixation, unstable microtubules were disassembled using Ca^{2+}-containing buffer (1 mM $MgCl_2$, 1 mM $CaCl_2$, 0.5% Triton X-100, and 100 mM Pipes, pH 6.8) for 1 min at 37°C. Fixed cells were incubated with primary antibodies for 1 h, washed with PBS supplemented with 0.02% Triton X-100, and incubated with secondary antibodies coupled with Alexa Fluor–488/568/594/647 (Thermo Fisher Scientific; A11029/A11032 for mouse IgG, A11034/A11037/A32733 for rabbit IgG, and A21090 for human IgG; 1:3,000) and/or DyLight-350 (Thermo Fisher Scientific; 62273 for mouse IgG, 1:3,000) for 1 h. Antibody incubations were performed in PBS supplemented with 0.02% Triton X-100. After final washes, cells were mounted with ProLong Gold (Thermo Fisher Scientific). Z-image stacks were captured in 0.2-µm increments on an Olympus IX-71 inverted microscope controlled by DeltaVision softWoRx (Cytiva) using ×100 1.40 NA Plan Apochromat oil objective lens (Olympus) with a CoolSnapHQ2 charge-coupled device camera (Photometrics). Deconvolution was performed when necessary using enhanced ratio algorithm, medium noise filtering, and 10 iterations per channel. Image stacks were projected and saved as TIFF files and Photoshop files. In Fig. S5 K, magnified image stacks were projected with five Z-sections and used for quantification. All cells analyzed were selected from nonoverlapping fields. For quantification of the Hec1-S55 and -S69 phosphorylation signals, signal intensity of the area overlapping with the Hec1 signal was quantified. The signal of the same area at the cytoplasm was subtracted as background signal. Each experiment was successfully repeated at least three times.

Fluorescence in situ hybridization (FISH) analysis

Cells were grown on a glass coverslip and hypotonically swollen in PBS diluted to 20% with tap water for 5 min. Cells were fixed with methanol–acetic acid (3:1) for 5 min and then dried. The coverslip was hardened for 2 h at 70°C. Fixed cells were denatured with 70% formamide in 2×SSC (300 mM NaCl and 30 mM $C_6H_5Na_3O_7$-$2H_2O$, pH 7.0) for 2 min at 70°C, washed with ethanol, and dried. Denatured cells were incubated with predenatured FISH probes for centromeres of chromosome 7 and 12 (Vysis CEP 7 [D7Z1] SpectrumOrange probe and Vysis CEP 12 [D12Z3] SpectrumGreen probe, respectively; Abbott) in CEP Hybridization Buffer (Abbott) for 12 h at 37°C and washed with 50% formamide in 2×SSC and 1×SSC with DAPI. After final washes, cells were mounted with ProLong Gold (Thermo Fisher Scientific). Z-image stacks were captured in 0.2-µm increments on an Olympus IX-71 inverted microscope controlled by DeltaVision softWoRx using ×20 0.75 NA UPLSAPO objective lens (Olympus) with a CoolSnapHQ2 charge-coupled device camera. Image stacks were projected and saved as TIFF files. Fluorescence foci on the DAPI signal were counted using Speckle Inspector of BioVoxxel ToolBox plug-in (http://www.biovoxxel.de/) for Fiji (Schindelin et al., 2012). All cells analyzed were selected from nonoverlapping fields. Each experiment was successfully repeated at least three times.

WB

Cells were lysed in TNE-N buffer (1% NP-40, 100 mM NaCl, 10 mM Tris-HCl, pH 7.5, and 1 mM EDTA). Protein concentration in the cell lysate was measured using the Bio-Rad Protein assay kit. Cell lysates were boiled for 10 min with 4×NuPAGE LDS sample buffer (Thermo Fisher Scientific). Proteins were separated using the NuPAGE SDS gel system (Thermo Fisher Scientific), electroblotted onto a polyvinylidene difluoride membrane (Amersham Hybond-P; GE Healthcare Life Sciences), and subjected to immunodetection using appropriate primary antibodies. Blocking and antibody incubations were performed in 3% nonfat dry milk. Proteins were visualized using horseradish peroxidase–labeled secondary antibodies (Santa Cruz

Biotechnology; 1:3,000) and enhanced chemiluminescence using ECL prime Western Blotting Detection Reagents (GE Healthcare Life Sciences) according to the manufacturer's instructions.

Live-cell imaging

An EGFP–CENP-A–expressing U2OS cell and EGFP–CENP-A/EGFP–α-tubulin–expressing RPE-1 cell, HeLa cell, HCT116 cell, and MCF-7 cell were used. For TIG-3 cells, HCT-15 cells, DLD-1 cells, DU145 cells, and Aurora A–mAID-mClover cells, an expression plasmid for EGFP–CENP-A was transfected using the Neon Transfection System (Thermo Fisher Scientific). For A549 cells, a lentiviral vector coding for EGFP–CENP-A was infected for 48 h before imaging. Cells were treated with CellLight Tubulin–GFP (Thermo Fisher Scientific) for 24 h or SiR-Tubulin (Spirochrome) for 6 h before imaging. Neon Transfection System (Thermo Fisher Scientific), ViraSafe Lentiviral Bicistronic Expression System (Cell Biolabs), CellLight Tubulin–GFP (Thermo Fisher Scientific), and SiR-Tubulin (Cytoskeleton, Inc.) were used according to the manufactures' instructions. Cells were grown in glass chambers (Thermo Fisher Scientific). 1 h before imaging, the medium was changed to prewarmed Leibovitz's L-15 medium (Thermo Fisher Scientific) supplemented with 20% fetal bovine serum. Recordings were made in a temperature-controlled incubator at 37°C, as described previously (Itoh et al., 2018; Itoh et al., 2011). Z-series of five sections in 0.5-µm increments were captured every 2 s, except for Fig. S1 A, where images were captured every 5 s. Image stacks were projected with three Z-sections and used for tracking. Kinetochore positions and spindle edges were tracked in deconvolved movies using the StackReg (Thévenaz et al., 1998) and Manual Tracking (http://rsb.info.nih.gov/ij/plugins/track/track.html) plug-ins for Fiji (Schindelin et al., 2012). The spindle lengths in all images were adjusted to 60 pixels (7.7 µm), and kinetochore to equator distance was normalized by the adjusted value of spindle length at each time point according to the previous study (Iemura and Tanaka, 2015). The DAP was determined using Microsoft Excel as previously described (Stumpff et al., 2008). All time-lapse images were collected with an Olympus IX-71 inverted microscope controlled by DeltaVision softWoRx using a ×100 1.40 NA Plan Apochromat oil objective lens with a CoolSnapHQ2 charge-coupled device camera. Deconvolution was performed when necessary using enhanced ratio algorithm, medium noise filtering, and 10 iterations per channel.

Statistical analysis

The Mann–Whitney *U* test was used for comparison of dispersion, and a two-sided *t* test was used for comparisons of average. A two-sided F-test validated the dispersibility of each category before the Student's *t* test. If the result of the F-test was an unequal variance, a significant difference between samples was validated by a two-sided Welch's *t* test. For comparisons between all groups showing normal distribution, a one-way ANOVA test was used with the Tukey–Kramer post hoc test. The Kolmogorov–Smirnov test verified the normality of data distribution for each group before the one-way ANOVA test. If the result of the Kolmogorov–Smirnov test was nonnominal distribution, the significant differences between all groups were validated by the Kruskal–Wallis test, which was used with Steel–Dwass post hoc test. For comparisons between the single group and multi groups showing normal distribution, Dunnett's post hoc test was used after a one-way ANOVA test. If the result of the Kolmogorov–Smirnov test was nonnominal distribution, the significant differences between single group and multi groups were validated by a Steel post hoc test after the Kruskal–Wallis test. All statistical analyses were performed with EZR (Kanda, 2013), which is a graphical user interface for R (R Core Team, 2018). More precisely, it is a modified version of R commander designed to add statistical functions frequently used in biostatistics. Samples for analysis in each dataset were acquired in the same experiment, and all samples were calculated at the same time for each dataset.

Online supplemental material

Fig. S1 shows chromosome oscillation in RPE-1 and HeLa cells in the absence of MG132, quantification of cells containing micronuclei and the number of FISH signals, variance of kinetochore-spindle equator distance, spindle length, cell size, and interkinetochore distance in nontransformed and cancer cell lines. Fig. S2 illustrates Hec1-S55 phosphorylation in RPE-1 and HeLa cells in the presence of a blocking peptide or Calyculin A, Hec1-S55 phosphorylation in RPE-1 cells after Hec1 RNAi with or without expression of Hec1-GFP constructs, Hec1-S69 phosphorylation in HeLa and RPE-1 cells during prometaphase and metaphase, and Hec1-S69 phosphorylation in nontransformed and cancer cell lines. Fig. S3 depicts depletion of Aurora A/B–mAID-mClover by adding IAA in RPE-1 cells, Hec1-S55 phosphorylation in RPE-1 cells arrested in metaphase depleted of Aurora B using the AID system, and Hec1-S55 and -S69 phosphorylation in RPE-1 cells depleted of INCENP. Fig. S4 depicts depletion of mAID-mClover-TPX2 by adding IAA in RPE-1 cells, Hec1-S55 phosphorylation and Aurora A–T288 phosphorylation in RPE-1 cells arrested in metaphase expressing Aurora A mutants, and Aurora A distribution on the spindle during prometaphase and metaphase. Fig. S5 shows chromosome oscillation in HeLa cells in the presence of BTB-1 or Calyculin A, Hec1-S55 phosphorylation in HeLa cells in the presence of BTB-1, Hec1-S69 phosphorylation in HeLa cells in the presence of BTB-1 or UMK57, expression of Hec1–GFP constructs in RPE-1 cells depleted of endogenous Hec1, quantification of the kinetochore pairs forming merotelic attachment in HeLa and RPE-1 cells, spindle structure and amount of spindle microtubules in the presence of Aurora inhibitors, and expression of Aurora A and TPX2 in nontransformed and cancer cell lines. Video 1 shows live-cell imaging of chromosome oscillation in RPE-1 and HeLa cells. Video 2 shows live-cell imaging of chromosome motion in RPE-1 and HeLa cells in the absence of MG132. Video 3 shows live-cell imaging of chromosome oscillation in TIG3, HCT-15, DLD-1, HCT116, DU145, A549, U2OS, and MCF-7 cells. Video 4 shows live-cell imaging of chromosome oscillation in RPE-1 or HeLa cells treated with taxol, BTB-1, and UMK57 or depleted of Kif18A. Video 5 shows live-cell imaging of chromosome oscillation in RPE-1 cells treated with AZD1152 or MLN8237, Aurora A–mAID-mClover–expressing RPE-1 cells treated with DMSO or IAA, and a HeLa cell treated with Calyculin A. Video 6 shows

live-cell imaging of chromosome oscillation in RPE-1 cells expressing Hec1-WT, Hec1-S55A, Hec1-S69A, Hec1-2A, Hec1-8A-S55WT, Hec1-8A-S69WT, or Hec1-7A-2WT depleted of endogenous Hec1.

Acknowledgments

The authors thank J.G. DeLuca for the Hec1 constructs mutated at the phosphorylation sites and the antibody against phosphorylated Hec1-S69, P. Wadsworth for an mCherry-TPX2 expression plasmid, F. Zhang for a guide RNA expression plasmid, H. Hochegger for the RPE-1 cell line, and T. Hirota for HeLa Kyoto and U2OS cell lines. We also thank members of the K. Tanaka laboratory for discussions and A. Harata for technical assistance.

This work was supported by the Japan Society for the Promotion of Science KAKENHI grant nos. 26640067, 15H04368, 16K14604, and 18H02434; Ministry of Education, Culture, Sports, Science, and Technology KAKENHI grant nos. 26114702 and 18H04896; grants from the Takeda Science Foundation and National Institute of Genetics-JOINT (2016-A1-25) to K. Tanaka; the Japan Society for the Promotion of Science KAKENHI grant nos. 16H06635 and 18K15234; and Uehara Memorial Foundation, Kanae Foundation for the Promotion of Medical Science, and Gonryo Medical Foundation for K. Iemura.

The authors declare no competing financial interests.

Author contributions: K. Iemura and K. Tanaka designed the experiments. K. Iemura, T. Natsume, K. Maehara, and M.T. Kanemaki performed the experiments. K. Iemura and K. Tanaka wrote the manuscript. K. Tanaka supervised the work.

Submitted: 19 June 2020
Revised: 10 March 2021
Accepted: 21 April 2021

References

Abe, Y., K. Sako, K. Takagaki, Y. Hirayama, K.S. Uchida, J.A. Herman, J.G. DeLuca, and T. Hirota. 2016. HP1-Assisted Aurora B Kinase Activity Prevents Chromosome Segregation Errors. *Dev. Cell.* 36:487–497. https://doi.org/10.1016/j.devcel.2016.02.008

Asai, Y., K. Fukuchi, Y. Tanno, S. Koitabashi-Kiyozuka, T. Kiyozuka, Y. Noda, R. Matsumura, T. Koizumi, A. Watanabe, K. Nagata, et al. 2019. Aurora B kinase activity is regulated by SET/TAF1 on Sgo2 at the inner centromere. *J. Cell Biol.* 218:3223–3236. https://doi.org/10.1083/jcb.201811060

Bakhoum, S.F., and D.A. Compton. 2012a. Chromosomal instability and cancer: a complex relationship with therapeutic potential. *J. Clin. Invest.* 122:1138–1143. https://doi.org/10.1172/JCI59954

Bakhoum, S.F., and D.A. Compton. 2012b. Kinetochores and disease: keeping microtubule dynamics in check! *Curr. Opin. Cell Biol.* 24:64–70. https://doi.org/10.1016/j.ceb.2011.11.012

Bakhoum, S.F., G. Genovese, and D.A. Compton. 2009a. Deviant kinetochore microtubule dynamics underlie chromosomal instability. *Curr. Biol.* 19:1937–1942. https://doi.org/10.1016/j.cub.2009.09.055

Bakhoum, S.F., S.L. Thompson, A.L. Manning, and D.A. Compton. 2009b. Genome stability is ensured by temporal control of kinetochore-microtubule dynamics. *Nat. Cell Biol.* 11:27–35. https://doi.org/10.1038/ncb1809

Bayliss, R., T. Sardon, I. Vernos, and E. Conti. 2003. Structural basis of Aurora-A activation by TPX2 at the mitotic spindle. *Mol. Cell.* 12:851–862. https://doi.org/10.1016/S1097-2765(03)00392-7

Ben-David, U., and A. Amon. 2020. Context is everything: aneuploidy in cancer. *Nat. Rev. Genet.* 21:44–62. https://doi.org/10.1038/s41576-019-0171-x

Bibby, R.A., C. Tang, A. Faisal, K. Drosopoulos, S. Lubbe, R. Houlston, R. Bayliss, and S. Linardopoulos. 2009. A cancer-associated aurora A mutant is mislocalized and misregulated due to loss of interaction with TPX2. *J. Biol. Chem.* 284:33177–33184. https://doi.org/10.1074/jbc.M109.032722

Bischoff, J.R., L. Anderson, Y. Zhu, K. Mossie, L. Ng, B. Souza, B. Schryver, P. Flanagan, F. Clairvoyant, C. Ginther, et al. 1998. A homologue of Drosophila aurora kinase is oncogenic and amplified in human colorectal cancers. *EMBO J.* 17:3052–3065. https://doi.org/10.1093/emboj/17.11.3052

Bucko, P.J., C.K. Lombard, L. Rathbun, I. Garcia, A. Bhat, L. Wordeman, F.D. Smith, D.J. Maly, H. Hehnly, and J.D. Scott. 2019. Subcellular drug targeting illuminates local kinase action. *eLife.* 8:e52220. https://doi.org/10.7554/eLife.52220

Catarinella, M., T. Grüner, T. Strittmatter, A. Marx, and T.U. Mayer. 2009. BTB-1: a small molecule inhibitor of the mitotic motor protein Kif18A. *Angew. Chem. Int. Ed. Engl.* 48:9072–9076. https://doi.org/10.1002/anie.200904510

Chmátal, L., K. Yang, R.M. Schultz, and M.A. Lampson. 2015. Spatial Regulation of Kinetochore Microtubule Attachments by Destabilization at Spindle Poles in Meiosis I. *Curr. Biol.* 25:1835–1841. https://doi.org/10.1016/j.cub.2015.05.013

Cimini, D. 2008. Merotelic kinetochore orientation, aneuploidy, and cancer. *Biochim. Biophys. Acta.* 1786:32–40.

Cimini, D., X. Wan, C.B. Hirel, and E.D. Salmon. 2006. Aurora kinase promotes turnover of kinetochore microtubules to reduce chromosome segregation errors. *Curr. Biol.* 16:1711–1718. https://doi.org/10.1016/j.cub.2006.07.022

Cong, L., F.A. Ran, D. Cox, S. Lin, R. Barretto, N. Habib, P.D. Hsu, X. Wu, W. Jiang, L.A. Marraffini, and F. Zhang. 2013. Multiplex genome engineering using CRISPR/Cas systems. *Science.* 339:819–823. https://doi.org/10.1126/science.1231143

DeLuca, J.G., W.E. Gall, C. Ciferri, D. Cimini, A. Musacchio, and E.D. Salmon. 2006. Kinetochore microtubule dynamics and attachment stability are regulated by Hec1. *Cell.* 127:969–982. https://doi.org/10.1016/j.cell.2006.09.047

DeLuca, K.F., S.M. Lens, and J.G. DeLuca. 2011. Temporal changes in Hec1 phosphorylation control kinetochore-microtubule attachment stability during mitosis. *J. Cell Sci.* 124:622–634. https://doi.org/10.1242/jcs.072629

DeLuca, K.F., A. Meppelink, A.J. Broad, J.E. Mick, O.B. Peersen, S. Pektas, S.M.A. Lens, and J.G. DeLuca. 2018. Aurora A kinase phosphorylates Hec1 to regulate metaphase kinetochore-microtubule dynamics. *J. Cell Biol.* 217:163–177. https://doi.org/10.1083/jcb.201707160

Dodson, C.A., and R. Bayliss. 2012. Activation of Aurora-A kinase by protein partner binding and phosphorylation are independent and synergistic. *J. Biol. Chem.* 287:1150–1157. https://doi.org/10.1074/jbc.M111.312090

Eyers, P.A., E. Erikson, L.G. Chen, and J.L. Maller. 2003. A novel mechanism for activation of the protein kinase Aurora A. *Curr. Biol.* 13:691–697. https://doi.org/10.1016/S0960-9822(03)00166-0

Ferreira, L.T., B. Orr, G. Rajendraprasad, A.J. Pereira, C. Lemos, J.T. Lima, C. Guasch Boldú, J.G. Ferreira, M. Barisic, and H. Maiato. 2020. α-Tubulin detyrosination impairs mitotic error correction by suppressing MCAK centromeric activity. *J. Cell Biol.* 219:e201910064. https://doi.org/10.1083/jcb.201910064

Fonseca, C.L., H.L.H. Malaby, L.A. Sepaniac, W. Martin, C. Byers, A. Czechanski, D. Messinger, M. Tang, R. Ohi, L.G. Reinholdt, and J. Stumpff. 2019. Mitotic chromosome alignment ensures mitotic fidelity by promoting interchromosomal compaction during anaphase. *J. Cell Biol.* 218:1148–1163. https://doi.org/10.1083/jcb.201807228

Giubettini, M., I.A. Asteriti, J. Scrofani, M. De Luca, C. Lindon, P. Lavia, and G. Guarguaglini. 2011. Control of Aurora-A stability through interaction with TPX2. *J. Cell Sci.* 124:113–122. https://doi.org/10.1242/jcs.075457

Godek, K.M., L. Kabeche, and D.A. Compton. 2015. Regulation of kinetochore-microtubule attachments through homeostatic control during mitosis. *Nat. Rev. Mol. Cell Biol.* 16:57–64. https://doi.org/10.1038/nrm3916

Gordon, D.J., B. Resio, and D. Pellman. 2012. Causes and consequences of aneuploidy in cancer. *Nat. Rev. Genet.* 13:189–203. https://doi.org/10.1038/nrg3123

Guimaraes, G.J., Y. Dong, B.F. McEwen, and J.G. Deluca. 2008. Kinetochore-microtubule attachment relies on the disordered N-terminal tail domain of Hec1. *Curr. Biol.* 18:1778–1784. https://doi.org/10.1016/j.cub.2008.08.012

Häfner, J., M.I. Mayr, M.M. Möckel, and T.U. Mayer. 2014. Pre-anaphase chromosome oscillations are regulated by the antagonistic activities

of Cdk1 and PP1 on Kif18A. *Nat. Commun.* 5:4397. https://doi.org/10.1038/ncomms5397

Hauf, S., R.W. Cole, S. LaTerra, C. Zimmer, G. Schnapp, R. Walter, A. Heckel, J. van Meel, C.L. Rieder, and J.M. Peters. 2003. The small molecule Hesperadin reveals a role for Aurora B in correcting kinetochore-microtubule attachment and in maintaining the spindle assembly checkpoint. *J. Cell Biol.* 161:281–294. https://doi.org/10.1083/jcb.200208092

Hayashi, K., J. Neve, M. Hirose, A. Kuboki, Y. Shimada, S. Kepinski, and H. Nozaki. 2012. Rational design of an auxin antagonist of the SCF(TIR1) auxin receptor complex. *ACS Chem. Biol.* 7:590–598. https://doi.org/10.1021/cb200404c

Hoar, K., A. Chakravarty, C. Rabino, D. Wysong, D. Bowman, N. Roy, and J.A. Ecsedy. 2007. MLN8054, a small-molecule inhibitor of Aurora A, causes spindle pole and chromosome congression defects leading to aneuploidy. *Mol. Cell. Biol.* 27:4513–4525. https://doi.org/10.1128/MCB.02364-06

Hochegger, H., N. Hégarat, and J.B. Pereira-Leal. 2013. Aurora at the pole and equator: overlapping functions of Aurora kinases in the mitotic spindle. *Open Biol.* 3:120185. https://doi.org/10.1098/rsob.120185

Holland, A.J., and D.W. Cleveland. 2012. Losing balance: the origin and impact of aneuploidy in cancer. *EMBO Rep.* 13:501–514. https://doi.org/10.1038/embor.2012.55

Iemura, K., and K. Tanaka. 2015. Chromokinesin Kid and kinetochore kinesin CENP-E differentially support chromosome congression without end-on attachment to microtubules. *Nat. Commun.* 6:6447. https://doi.org/10.1038/ncomms7447

Ishihara, H., B.L. Martin, D.L. Brautigan, H. Karaki, H. Ozaki, Y. Kato, N. Fusetani, S. Watabe, K. Hashimoto, D. Uemura, et al. 1989. Calyculin A and okadaic acid: inhibitors of protein phosphatase activity. *Biochem. Biophys. Res. Commun.* 159:871–877. https://doi.org/10.1016/0006-291X(89)92189-X

Itoh, G., S. Kanno, K.S. Uchida, S. Chiba, S. Sugino, K. Watanabe, K. Mizuno, A. Yasui, T. Hirota, and K. Tanaka. 2011. CAMP (C13orf8, ZNF828) is a novel regulator of kinetochore-microtubule attachment. *EMBO J.* 30:130–144. https://doi.org/10.1038/emboj.2010.276

Itoh, G., M. Ikeda, K. Iemura, M.A. Amin, S. Kuriyama, M. Tanaka, N. Mizuno, H. Osakada, T. Haraguchi, and K. Tanaka. 2018. Lateral attachment of kinetochores to microtubules is enriched in prometaphase rosette and facilitates chromosome alignment and bi-orientation establishment. *Sci. Rep.* 8:3888. https://doi.org/10.1038/s41598-018-22164-5

Jaqaman, K., E.M. King, A.C. Amaro, J.R. Winter, J.F. Dorn, H.L. Elliott, N. McHedlishvili, S.E. McClelland, I.M. Porter, M. Posch, et al. 2010. Kinetochore alignment within the metaphase plate is regulated by centromere stiffness and microtubule depolymerases. *J. Cell Biol.* 188:665–679. https://doi.org/10.1083/jcb.200909005

Kabeche, L., and D.A. Compton. 2013. Cyclin A regulates kinetochore microtubules to promote faithful chromosome segregation. *Nature.* 502:110–113. https://doi.org/10.1038/nature12507

Kanda, Y. 2013. Investigation of the freely available easy-to-use software 'EZR' for medical statistics. *Bone Marrow Transplant.* 48:452–458. https://doi.org/10.1038/bmt.2012.244

Ke, K., J. Cheng, and A.J. Hunt. 2009. The distribution of polar ejection forces determines the amplitude of chromosome directional instability. *Curr. Biol.* 19:807–815. https://doi.org/10.1016/j.cub.2009.04.036

Kim, Y., A.J. Holland, W. Lan, and D.W. Cleveland. 2010. Aurora kinases and protein phosphatase 1 mediate chromosome congression through regulation of CENP-E. *Cell.* 142:444–455. https://doi.org/10.1016/j.cell.2010.06.039

Koffa, M.D., C.M. Casanova, R. Santarella, T. Köcher, M. Wilm, and I.W. Mattaj. 2006. HURP is part of a Ran-dependent complex involved in spindle formation. *Curr. Biol.* 16:743–754. https://doi.org/10.1016/j.cub.2006.03.056

Kufer, T.A., H.H. Silljé, R. Körner, O.J. Gruss, P. Meraldi, and E.A. Nigg. 2002. Human TPX2 is required for targeting Aurora-A kinase to the spindle. *J. Cell Biol.* 158:617–623. https://doi.org/10.1083/jcb.200204155

Lampson, M.A., and I.M. Cheeseman. 2011. Sensing centromere tension: Aurora B and the regulation of kinetochore function. *Trends Cell Biol.* 21:133–140. https://doi.org/10.1016/j.tcb.2010.10.007

Long, A.F., D.B. Udy, and S. Dumont. 2017. Hec1 Tail Phosphorylation Differentially Regulates Mammalian Kinetochore Coupling to Polymerizing and Depolymerizing Microtubules. *Curr. Biol.* 27:1692–1699.e3. https://doi.org/10.1016/j.cub.2017.04.058

Ma, N., U.S. Tulu, N.P. Ferenz, C. Fagerstrom, A. Wilde, and P. Wadsworth. 2010. Poleward transport of TPX2 in the mammalian mitotic spindle requires dynein, Eg5, and microtubule flux. *Mol. Biol. Cell.* 21:979–988. https://doi.org/10.1091/mbc.e09-07-0601

Magidson, V., C.B. O'Connell, J. Lončarek, R. Paul, A. Mogilner, and A. Khodjakov. 2011. The spatial arrangement of chromosomes during prometaphase facilitates spindle assembly. *Cell.* 146:555–567. https://doi.org/10.1016/j.cell.2011.07.012

Manfredi, M.G., J.A. Ecsedy, K.A. Meetze, S.K. Balani, O. Burenkova, W. Chen, K.M. Galvin, K.M. Hoar, J.J. Huck, P.J. LeRoy, et al. 2007. Antitumor activity of MLN8054, an orally active small-molecule inhibitor of Aurora A kinase. *Proc. Natl. Acad. Sci. USA.* 104:4106–4111. https://doi.org/10.1073/pnas.0608798104

Mangal, S., J. Sacher, T. Kim, D.S. Osório, F. Motegi, A.X. Carvalho, K. Oegema, and E. Zanin. 2018. TPXL-1 activates Aurora A to clear contractile ring components from the polar cortex during cytokinesis. *J. Cell Biol.* 217:837–848. https://doi.org/10.1083/jcb.201706021

Mayr, M.I., S. Hümmer, J. Bormann, T. Grüner, S. Adio, G. Woehlke, and T.U. Mayer. 2007. The human kinesin Kif18A is a motile microtubule depolymerase essential for chromosome congression. *Curr. Biol.* 17:488–498. https://doi.org/10.1016/j.cub.2007.02.036

Mortlock, A.A., K.M. Foote, N.M. Heron, F.H. Jung, G. Pasquet, J.J. Lohmann, N. Warin, F. Renaud, C. De Savi, N.J. Roberts, et al. 2007. Discovery, synthesis, and in vivo activity of a new class of pyrazoloquinazolines as selective inhibitors of aurora B kinase. *J. Med. Chem.* 50:2213–2224. https://doi.org/10.1021/jm061335f

Natsume, T., T. Kiyomitsu, Y. Saga, and M.T. Kanemaki. 2016. Rapid Protein Depletion in Human Cells by Auxin-Inducible Degron Tagging with Short Homology Donors. *Cell Rep.* 15:210–218. https://doi.org/10.1016/j.celrep.2016.03.001

Nishimura, K., T. Fukagawa, H. Takisawa, T. Kakimoto, and M. Kanemaki. 2009. An auxin-based degron system for the rapid depletion of proteins in nonplant cells. *Nat. Methods.* 6:917–922. https://doi.org/10.1038/nmeth.1401

Orr, B., L. Talje, Z. Liu, B.H. Kwok, and D.A. Compton. 2016. Adaptive Resistance to an Inhibitor of Chromosomal Instability in Human Cancer Cells. *Cell Rep.* 17:1755–1763. https://doi.org/10.1016/j.celrep.2016.10.030

R Core Team. 2018. R: A Language and Environment for Statistical Computing. https://www.R-project.org/

Sackton, K.L., N. Dimova, X. Zeng, W. Tian, M. Zhang, T.B. Sackton, J. Meaders, K.L. Pfaff, F. Sigoillot, H. Yu, et al. 2014. Synergistic blockade of mitotic exit by two chemical inhibitors of the APC/C. *Nature.* 514:646–649. https://doi.org/10.1038/nature13660

Salimian, K.J., E.R. Ballister, E.M. Smoak, S. Wood, T. Panchenko, M.A. Lampson, and B.E. Black. 2011. Feedback control in sensing chromosome biorientation by the Aurora B kinase. *Curr. Biol.* 21:1158–1165. https://doi.org/10.1016/j.cub.2011.06.015

Saurin, A.T. 2018. Kinase and Phosphatase Cross-Talk at the Kinetochore. *Front. Cell Dev. Biol.* 6:62. https://doi.org/10.3389/fcell.2018.00062

Schindelin, J., I. Arganda-Carreras, E. Frise, V. Kaynig, M. Longair, T. Pietzsch, S. Preibisch, C. Rueden, S. Saalfeld, B. Schmid, et al. 2012. Fiji: an open-source platform for biological-image analysis. *Nat. Methods.* 9:676–682. https://doi.org/10.1038/nmeth.2019

Schmidt, J.C., H. Arthanari, A. Boeszoermenyi, N.M. Dashkevich, E.M. Wilson-Kubalek, N. Monnier, M. Markus, M. Oberer, R.A. Milligan, M. Bathe, et al. 2012. The kinetochore-bound Ska1 complex tracks depolymerizing microtubules and binds to curved protofilaments. *Dev. Cell.* 23:968–980. https://doi.org/10.1016/j.devcel.2012.09.012

Skibbens, R.V., V.P. Skeen, and E.D. Salmon. 1993. Directional instability of kinetochore motility during chromosome congression and segregation in mitotic newt lung cells: a push-pull mechanism. *J. Cell Biol.* 122:859–875. https://doi.org/10.1083/jcb.122.4.859

Smith, R.J., M.H. Cordeiro, N.E. Davey, G. Vallardi, A. Ciliberto, F. Gross, and A.T. Saurin. 2019. PP1 and PP2A Use Opposite Phospho-dependencies to Control Distinct Processes at the Kinetochore. *Cell Rep.* 28:2206–2219.e8. https://doi.org/10.1016/j.celrep.2019.07.067

Stumpff, J., G. von Dassow, M. Wagenbach, C. Asbury, and L. Wordeman. 2008. The kinesin-8 motor Kif18A suppresses kinetochore movements to control mitotic chromosome alignment. *Dev. Cell.* 14:252–262. https://doi.org/10.1016/j.devcel.2007.11.014

Stumpff, J., M. Wagenbach, A. Franck, C.L. Asbury, and L. Wordeman. 2012. Kif18A and chromokinesins confine centromere movements via microtubule growth suppression and spatial control of kinetochore tension. *Dev. Cell.* 22:1017–1029. https://doi.org/10.1016/j.devcel.2012.02.013

Tanaka, T.U. 2002. Bi-orienting chromosomes on the mitotic spindle. *Curr. Opin. Cell Biol.* 14:365–371. https://doi.org/10.1016/S0955-0674(02)00328-9

Tanaka, K. 2013. Regulatory mechanisms of kinetochore-microtubule interaction in mitosis. *Cell. Mol. Life Sci.* 70:559–579. https://doi.org/10.1007/s00018-012-1057-7

Tanaka, K., and T. Hirota. 2016. Chromosomal instability: A common feature and a therapeutic target of cancer. *Biochim. Biophys. Acta.* 1866:64–75. https://doi.org/10.1016/j.bbcan.2016.06.002

Tanaka, T.U., M.J. Stark, and K. Tanaka. 2005. Kinetochore capture and bi-orientation on the mitotic spindle. *Nat. Rev. Mol. Cell Biol.* 6:929–942. https://doi.org/10.1038/nrm1764

Thévenaz, P., U.E. Ruttimann, and M. Unser. 1998. A pyramid approach to subpixel registration based on intensity. *IEEE Trans. Image Process.* 7: 27–41. https://doi.org/10.1109/83.650848

Tsai, M.Y., C. Wiese, K. Cao, O. Martin, P. Donovan, J. Ruderman, C. Prigent, and Y. Zheng. 2003. A Ran signalling pathway mediated by the mitotic kinase Aurora A in spindle assembly. *Nat. Cell Biol.* 5:242–248. https://doi.org/10.1038/ncb936

Wan, X., D. Cimini, L.A. Cameron, and E.D. Salmon. 2012. The coupling between sister kinetochore directional instability and oscillations in centromere stretch in metaphase PtK1 cells. *Mol. Biol. Cell.* 23: 1035–1046. https://doi.org/10.1091/mbc.e11-09-0767

Weaver, B.A., and D.W. Cleveland. 2006. Does aneuploidy cause cancer? *Curr. Opin. Cell Biol.* 18:658–667. https://doi.org/10.1016/j.ceb.2006.10.002

Wimbish, R.T., and J.G. DeLuca. 2020. Hec1/Ndc80 Tail Domain Function at the Kinetochore-Microtubule Interface. *Front. Cell Dev. Biol.* 8:43. https://doi.org/10.3389/fcell.2020.00043

Wong, J., and G. Fang. 2006. HURP controls spindle dynamics to promote proper interkinetochore tension and efficient kinetochore capture. *J. Cell Biol.* 173:879–891. https://doi.org/10.1083/jcb.200511132

Ye, A.A., J. Deretic, C.M. Hoel, A.W. Hinman, D. Cimini, J.P. Welburn, and T.J. Maresca. 2015. Aurora A Kinase Contributes to a Pole-Based Error Correction Pathway. *Curr. Biol.* 25:1842–1851. https://doi.org/10.1016/j.cub.2015.06.021

Yesbolatova, A., T. Natsume, K.I. Hayashi, and M.T. Kanemaki. 2019. Generation of conditional auxin-inducible degron (AID) cells and tight control of degron-fused proteins using the degradation inhibitor auxinole. *Methods.* 164-165:73–80. https://doi.org/10.1016/j.ymeth.2019.04.010

Yvon, A.M., P. Wadsworth, and M.A. Jordan. 1999. Taxol suppresses dynamics of individual microtubules in living human tumor cells. *Mol. Biol. Cell.* 10:947–959. https://doi.org/10.1091/mbc.10.4.947

Zaytsev, A.V., L.J. Sundin, K.F. DeLuca, E.L. Grishchuk, and J.G. DeLuca. 2014. Accurate phosphoregulation of kinetochore-microtubule affinity requires unconstrained molecular interactions. *J. Cell Biol.* 206:45–59. https://doi.org/10.1083/jcb.201312107

Zeng, X., F. Sigoillot, S. Gaur, S. Choi, K.L. Pfaff, D.C. Oh, N. Hathaway, N. Dimova, G.D. Cuny, and R.W. King. 2010. Pharmacologic inhibition of the anaphase-promoting complex induces a spindle checkpoint-dependent mitotic arrest in the absence of spindle damage. *Cancer Cell.* 18:382–395. https://doi.org/10.1016/j.ccr.2010.08.010

Zhang, R., J. Roostalu, T. Surrey, and E. Nogales. 2017. Structural insight into TPX2-stimulated microtubule assembly. *eLife.* 6:e30959. https://doi.org/10.7554/eLife.30959

Zorba, A., V. Buosi, S. Kutter, N. Kern, F. Pontiggia, Y.J. Cho, and D. Kern. 2014. Molecular mechanism of Aurora A kinase autophosphorylation and its allosteric activation by TPX2. *eLife.* 3:e02667. https://doi.org/10.7554/eLife.02667

JCB

Supplemental material

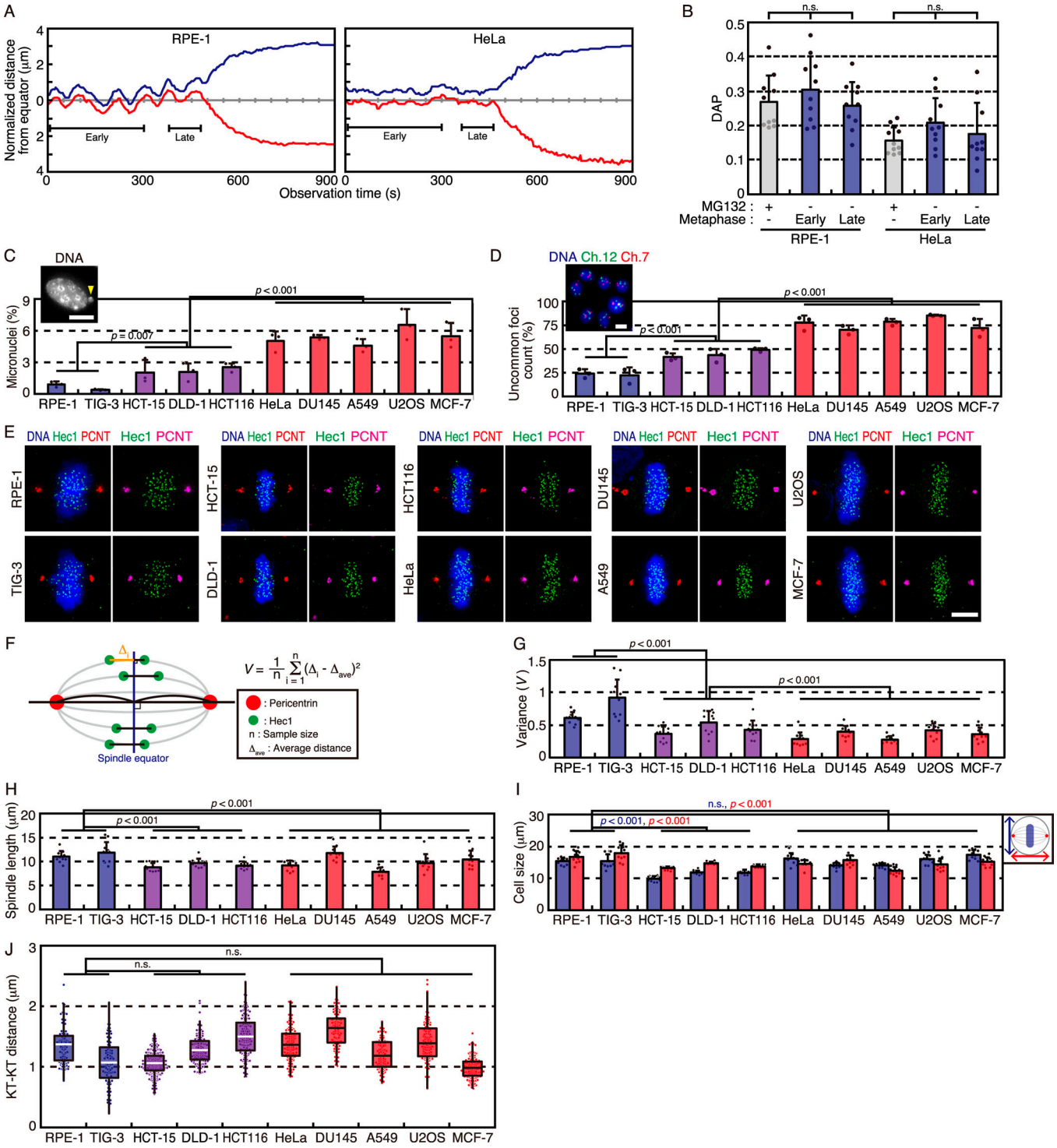

Figure S1. **Cancer cell lines show reduced displacement of kinetochores from the spindle equator during metaphase. (A)** Trajectories of kinetochores in RPE-1 and HeLa cells during unperturbed mitotic progression through metaphase to anaphase. The blue and red trajectories show the movements of a pair of sister kinetochores plotted as the distance from the spindle equator. **(B)** DAP measurements of kinetochore position in RPE-1 and HeLa cells during metaphase in the presence of MG132 or early and late metaphase without MG132 treatment. Error bars represent SD of 10 kinetochore pairs from three cells. P values were obtained using the Tukey–Kramer multiple comparisons test. **(C)** Quantification of cells containing micronuclei in nontransformed (blue), non-CIN (purple), and CIN (red) cancer cell lines. Cells were stained with DAPI after fixation, and interphase cells were observed for the presence of micronuclei (yellow arrowhead in the inset, scale bar: 5 μm). At least 223 cells were observed for each cell line. Error bars represent SD of three independent experiments. P values were obtained using the Tukey–Kramer multiple comparisons test. **(D)** Quantification of cells showing the number of FISH signals different from the modal number in nontransformed (blue), non-CIN (purple), and CIN (red) cancer cell lines. Cells were fixed and stained with FISH probes for chromosomes (Ch.) 7 and 12 (inset, scale bar: 10 μm). Modal number of FISH signals was determined for each probe in each cell line. At least 165 cells were observed for each cell line. Error bars represent SD of three independent experiments. P values were obtained using the Tukey–Kramer multiple comparisons test. **(E)** Immunostaining of

metaphase cells in nontransformed and cancer cell lines. Cells were treated with MG132 for 3 h and then fixed and stained with anti-Hec1 (green) and anti-pericentrin (PCNT; red) antibodies. DNA was stained with DAPI (blue). Scale bar: 5 µm. **(F)** Schematic diagram of quantifying variance (*V*) of kinetochore distance from the spindle equator during metaphase. **(G)** Quantification of variance of kinetochore distance from the spindle equator in nontransformed (blue), non-CIN (purple), and CIN (red) cancer cell lines during metaphase. Cells were treated as in E. The data represent the average variance of 10 cells, in which a minimum of 368 kinetochore pairs were quantified. Error bars represent SD. P values were obtained using the Tukey–Kramer multiple comparisons test. **(H)** Spindle length in metaphase cells. Cells were treated, fixed, and stained as in E, and spindle length in metaphase cells was measured as distance between pericentrin signals. 10 cells were observed for each cell line. Error bars represent SD. P values were obtained using the Tukey–Kramer multiple comparisons test. **(I)** Cell size in metaphase cells. Cells were treated, fixed, and stained as in E, and the diameters of metaphase cells, both longitudinal (blue) and parallel (red) to the spindle axes in bright field images, were measured. 10 cells were observed for each cell line. Error bars represent SD. P values were obtained using the Tukey–Kramer multiple comparisons test. **(J)** Interkinetochore distance in nontransformed (blue), non-CIN (purple), and CIN (red) cancer cell lines during metaphase. Cells were treated, fixed, and stained as in E, and interkinetochore distance was measured for a minimum of 102 sister kinetochore (KT) pairs from 10 cells for each cell line, displayed as box and dot plots. The bottom and top of the box show the lower and upper quartile values, respectively. The median is indicated with a bar in the box, and the whiskers denote the range within 1.5× size of the box. P values were obtained using the Steel–Dwass multiple comparisons test.

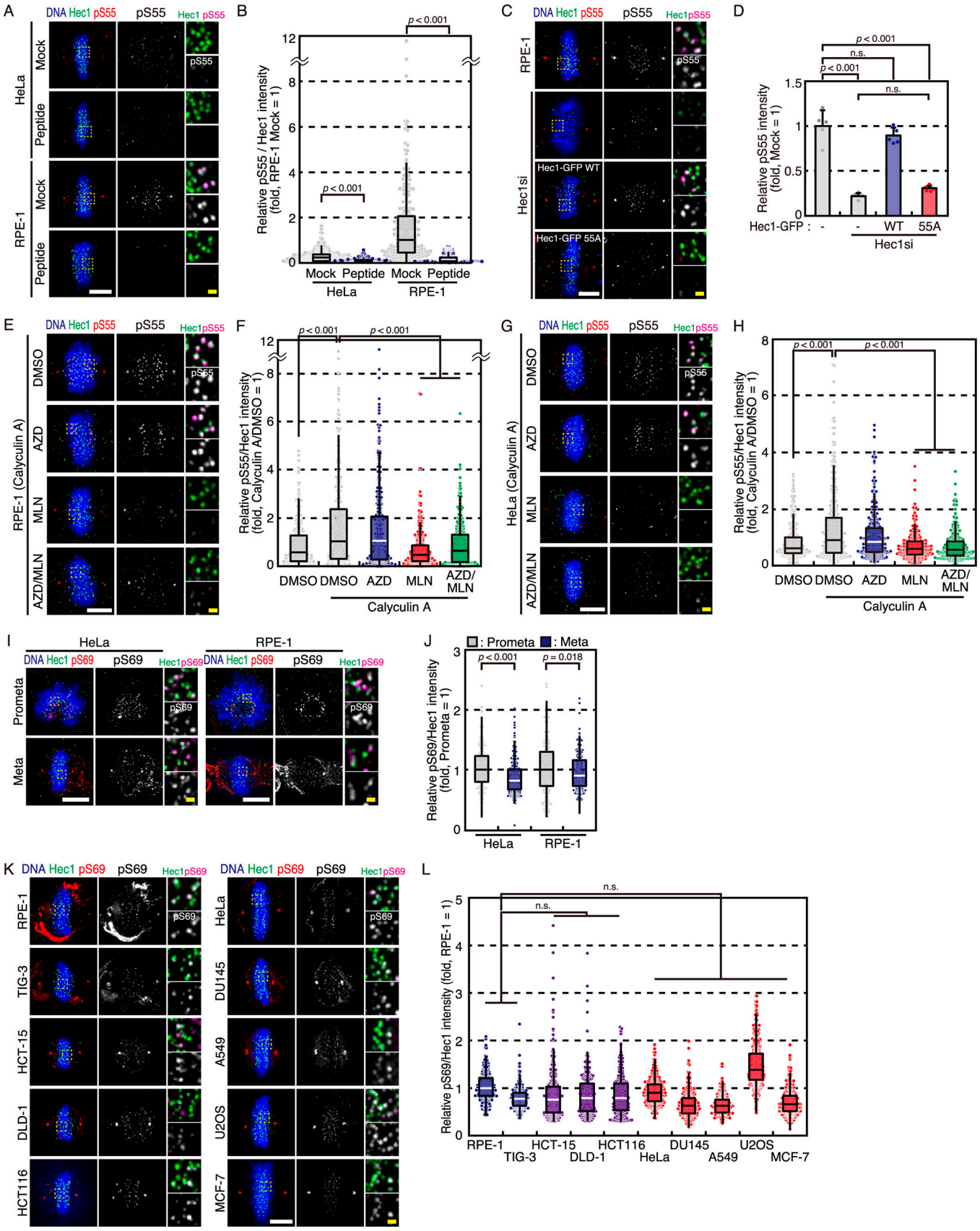

Figure S2. **Effect of a phosphatase inhibitor on the metaphase Hec1-S55 phosphorylation and Hec1-S69 phosphorylation in nontransformed and cancer cell lines. (A)** Specificity of Hec1-S55 phosphorylation signal in HeLa and RPE-1 cells in metaphase. Cells were arrested in metaphase in the presence of MG132, treated with a blocking peptide for anti–phospho-Hec1-S55 antibody, fixed, and stained with anti-Hec1 (green) and anti-phospho-Hec1-S55 (red) antibodies. DNA was stained with DAPI (blue). Boxed regions in the panels are shown as magnified images in insets. Scale bar: 5 µm (white), 500 nm (yellow).

(B) Quantification of phospho-Hec1-S55 signal in HeLa and RPE-1 cells in metaphase treated as in A. Relative intensity of the phosphorylated Hec1-S55 signal, which was calculated by dividing the phosphorylation signal with the Hec1 signal on each kinetochore, is displayed as box and dot plots as in Fig. 2 B. The median of mock-treated RPE-1 cells was set as 1. The data represent a minimum of 256 kinetochores from five cells for each condition. P values were obtained using the Mann–Whitney *U* test. **(C)** Specificity of Hec1-S55 phosphorylation signal in RPE-1 cells in metaphase. RPE-1 cells depleted of endogenous Hec1 and expressing EGFP-tagged WT Hec1 (WT) or Hec1-S55A, a phosphorylation site mutant, were arrested in metaphase by 2-h MG132 treatment and fixed and stained with anti-Hec1 (green) and anti–phospho-Hec1-S55 (red) antibodies. DNA was stained with DAPI (blue). Boxed regions in the panels are shown as magnified images in insets. Scale bar: 5 µm (white), 500 nm (yellow). **(D)** Quantification of phospho-Hec1-S55 signal in RPE-1 cells in metaphase treated as in C. Intensity of the phosphorylated Hec1-S55 signal on chromosomes is shown. The average of nontransfected RPE-1 cells was set as 1. Error bars represent SD of a minimum of five cells for each condition. P values were obtained using the Tukey–Kramer multiple comparisons test. **(E)** Hec1-S55 phosphorylation in RPE-1 cells during metaphase in the presence of Calyculin A. Cells were treated with Calyculin A and either DMSO or AZD1152 and/or MLN8237 for the last 1 h of the 3-h MG132 treatment, then fixed and stained with anti-Hec1 (green) and anti–phospho-Hec1-S55 (red) antibodies. DNA was stained with DAPI (blue). Cells arrested in metaphase are shown. Boxed regions in the panels are shown as magnified images in insets. Scale bar: 5 µm (white), 500 nm (yellow). **(F)** Quantification of the Hec1-S55 phosphorylation signal in RPE-1 cells during metaphase in the presence of Calyculin A. Relative intensity of the phospho-Hec1-S55 signal in cells treated as in E, which was calculated by dividing the phospho-Hec1-S55 signal with the Hec1 signal on each kinetochore, is displayed as box and dot plots as in Fig. 2 B. The median of Calyculin A–treated cells without Aurora inhibitors was set as 1. The data represent a minimum of 346 kinetochores from five cells for each condition. P values were obtained using the Steel multiple comparisons test. **(G)** Hec1-S55 phosphorylation in HeLa cells during metaphase in the presence of Calyculin A. Cells were treated as in E, then fixed and stained with anti-Hec1 (green) and anti–phospho-Hec1-S55 (red) antibodies. DNA was stained with DAPI (blue). Cells arrested in metaphase are shown. Boxed regions in the panels are shown as magnified images in insets. Scale bar: 5 µm (white), 500 nm (yellow). **(H)** Quantification of the Hec1-S55 phosphorylation signal in HeLa cells during metaphase in the presence of Calyculin A. Relative intensity of the phospho-Hec1-S55 signal in cells treated as in G, which was calculated as in F, is displayed as in Fig. 2 B. The median of Calyculin A–treated cells without Aurora inhibitors was set as 1. The data represent a minimum of 265 kinetochores from five cells for each condition. P values were obtained using the Steel multiple comparisons test. **(I)** Hec1-S69 phosphorylation in HeLa and RPE-1 cells during prometaphase (Prometa) and metaphase (Meta). Cells were fixed and stained with anti-Hec1 (green) and anti–phospho-Hec1-S69 (red) antibodies. DNA was stained with DAPI (blue). Boxed regions in the panels are shown as magnified images in insets. Scale bars: 5 µm (white), 500 nm (yellow). **(J)** Quantification of the Hec1-S69 phosphorylation signal in HeLa and RPE-1 cells during prometaphase and metaphase. Relative intensity of the phosphorylated Hec1-S69 signal was calculated by dividing the phosphorylation signal by the Hec1 signal on each kinetochore and displayed as in Fig. 2 B. The median of prometaphase in each cell line was set as 1. The data represent a minimum of 194 kinetochores from five cells for each condition. P values were obtained using the Mann–Whitney *U* test. **(K)** Hec1-S69 phosphorylation in nontransformed and cancer cell lines during metaphase. Cells were treated with MG132 for 3 h and then fixed and stained with anti-Hec1 (green) and anti–phospho-Hec1-S69 (red) antibodies. DNA was stained with DAPI (blue). Boxed regions in the panels are shown as magnified images in insets. Scale bars: 5 µm (white), 500 nm (yellow). **(L)** Quantification of the Hec1-S69 phosphorylation signal in nontransformed (blue), non-CIN (purple), and CIN (red) cancer cell lines during metaphase. Relative intensity of phospho-Hec1-S69 signal in cells treated as in K was calculated and displayed as box and dot plots as in Fig. 2 B. The median of RPE-1 cells was set as 1. The data represent a minimum of 251 kinetochores from five cells for each cell line. P values were obtained using the Steel–Dwass multiple comparisons test. Hec1si, treatment with an siRNA for Hec1.

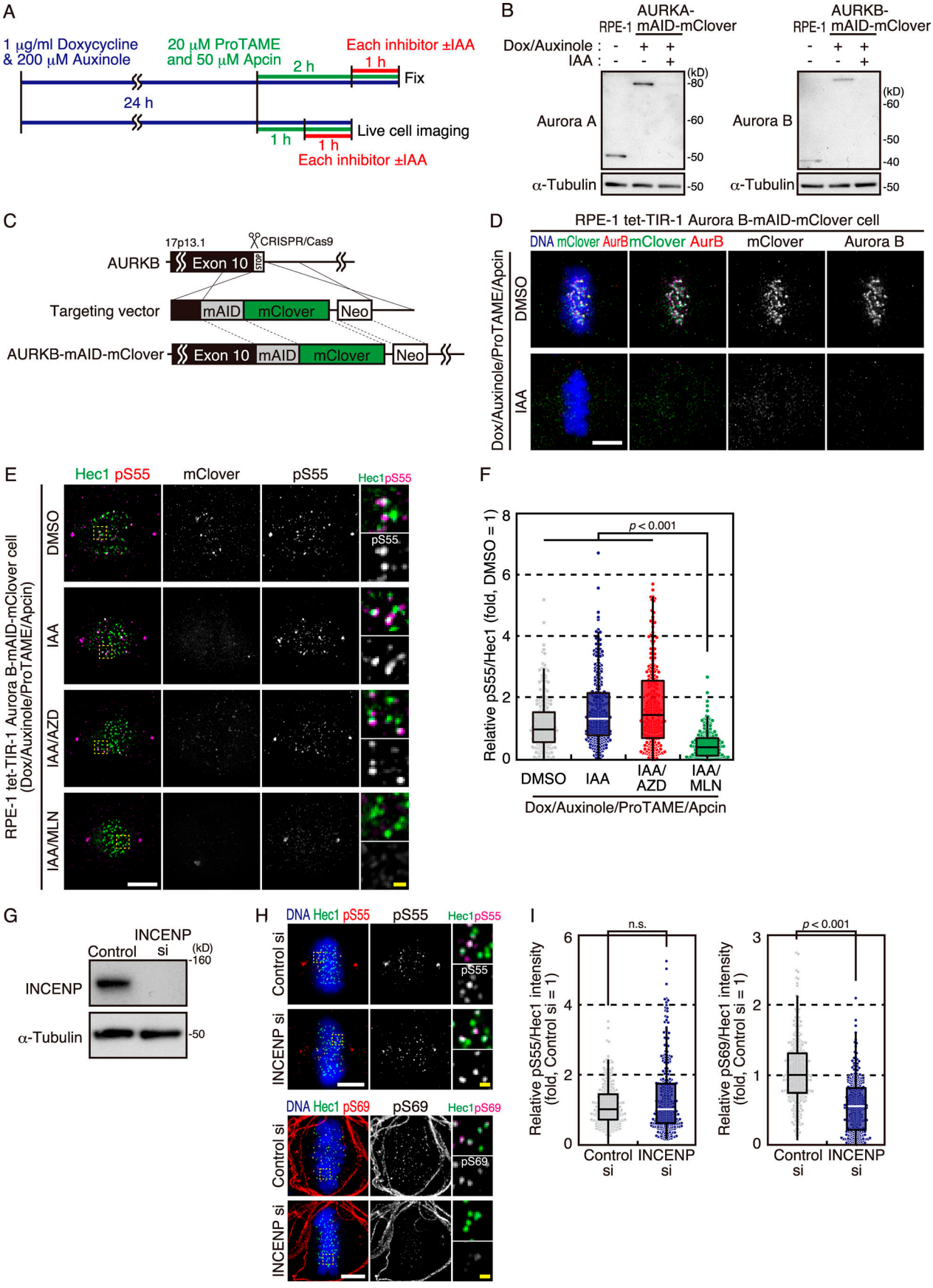

Figure S3. **Hec1-S55 phosphorylation in RPE-1 cells during metaphase is not dependent on Aurora B. (A)** Schematic of the procedure of experiments using cells expressing Aurora A/B–mAID-mClover or mAID-mClover-TPX2. **(B)** Depletion of Aurora A/B–mAID-mClover by adding IAA in RPE-1 cells arrested in metaphase. RPE-1 cells containing Aurora A/B–mAID-mClover were treated as in A, then harvested and lysed for immunoblot analysis using antibodies as indicated. Parental RPE-1 cells were used as a control. **(C)** Schematic diagram of tagging endogenous Aurora B with mAID-mClover tag by the CRISPR/Cas–based method. **(D)** Depletion of Aurora B–mAID-mClover by adding IAA to RPE-1 cells arrested in metaphase. Cells were treated as in A, then fixed and stained with an anti–Aurora B (AurB; red) antibody. DNA was stained with DAPI (blue). The mClover signal (green) was acquired by fluorescence microscopy. Cells arrested in metaphase are shown. Scale bar: 5 µm. **(E)** Hec1-S55 phosphorylation in RPE-1 cells arrested in metaphase depleted of Aurora B using the AID system. Cells treated as in A with or without AZD1152 and/or MLN8237 were fixed and stained with anti-Hec1 (blue, shown as green), and anti–phospho-Hec1-S55 (red) antibodies. The mClover signal (green, shown as monochrome) was acquired by fluorescence microscopy. Cells arrested in metaphase are shown. Boxed regions in the panels are shown as magnified images in insets. Scale bar: 5 µm (white), 500 nm (yellow). **(F)** Quantification of the Hec1-S55 phosphorylation signal in RPE-1 cells arrested in metaphase depleted of Aurora B using the AID system. Relative intensity of the phospho-Hec1-S55 signal in cells treated as in E was calculated and displayed as box and dot plots as in Fig. 2 B. The median of DMSO-treated cells was set as 1. The data represent a minimum of 245 kinetochores from five cells for each condition. P values were obtained using the Steel multiple comparisons test. **(G)** Efficiency of INCENP RNAi. Lysate of cells transfected with an siRNA against INCENP was subjected to immunoblot analysis using antibodies as indicated. **(H)** Hec1-S55 and -S69 phosphorylation in RPE-1 cells depleted of INCENP in metaphase. Cells were fixed and stained with anti-Hec1 (green) and anti–phospho-Hec1-S55 (upper panels, red) or -S69 (lower panels, red) antibodies. DNA was stained with DAPI (blue). Boxed regions in the panels are shown as magnified images in insets. Scale bars: 5 µm (white), 500 nm (yellow). **(I)** Quantification of the Hec1-S55 and -S69 phosphorylation signals in RPE-1 cells depleted of INCENP in metaphase. Relative intensity of the phosphorylated Hec1-S55 (left graph) or -S69 (right graph) signal was calculated by dividing the phosphorylation signal by the Hec1 signal on each kinetochore and displayed as in Fig. 2 B. The median of cells treated with control siRNA was set as 1. The data represent a minimum of 322 kinetochores from five cells for each condition. P values were obtained using the Mann–Whitney *U* test. AURKA, Aurora kinase A; AURKB, Aurora kinase B; Dox, doxycycline; Controlsi, treatment with a control siRNA; INCENPsi, treatment with an siRNA for INCENP.

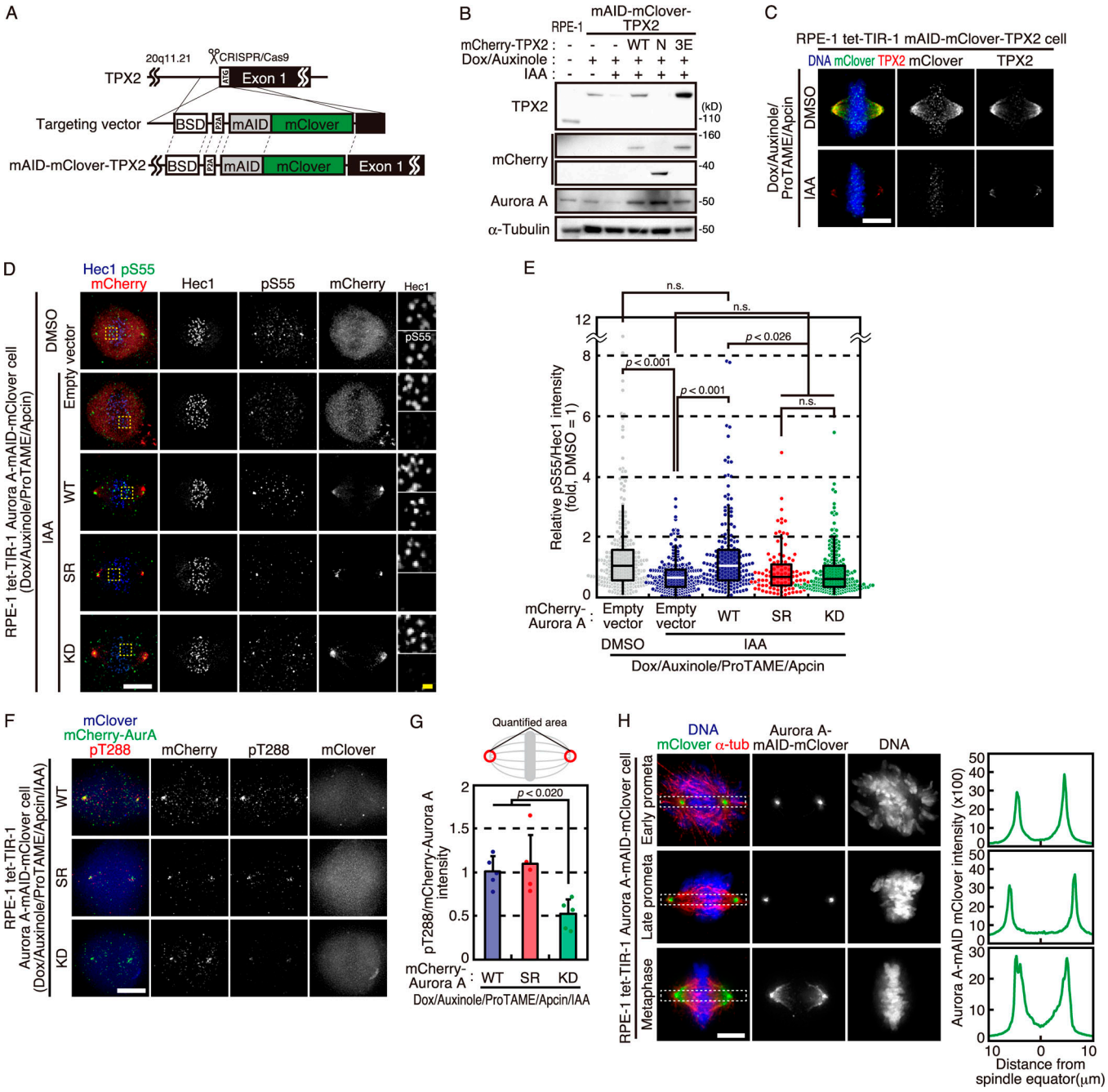

Figure S4. **Hec1-S55 phosphorylation in RPE-1 cells during metaphase is dependent on Aurora A residing at the spindle. (A)** Schematic diagram of tagging endogenous TPX2 with mAID-mClover tag by the CRISPR/Cas–based method. **(B)** Depletion of mAID-mClover-TPX2 by IAA and expression of TPX2 constructs in RPE-1 cells arrested in metaphase. RPE-1 cells containing mAID-mClover-TPX2 and stably expressing indicated TPX2 constructs were treated as in Fig. S3 A, then harvested and lysed for immunoblot analysis using antibodies as indicated. Parental RPE-1 cells were used as a control. **(C)** Depletion of mAID-mClover-TPX2 by adding IAA to RPE-1 cells arrested in metaphase. Cells were treated as in Fig. S3 A, then fixed and stained with anti-GFP (mClover, green) and anti-TPX2 (red) antibodies. DNA was stained with DAPI (blue). Cells arrested in metaphase are shown. Scale bar: 5 µm. **(D)** Hec1-S55 phosphorylation in RPE-1 cells arrested in metaphase expressing an Aurora A mutant that cannot localize to the spindle. RPE-1 cells containing Aurora A–mAID-mClover and expressing mCherry–Aurora A (WT, S155R [SR], or kinase-dead [KD]) were treated as in Fig. S3 A, then fixed and stained with anti-Hec1 (blue) and anti–phospho-Hec1-S55 (green) antibodies. The mCherry signal (red) was acquired by fluorescence microscopy. Cells arrested in metaphase are shown. Boxed regions in the panels are shown as magnified images in insets. Scale bar: 5 µm (white), 500 nm (yellow). **(E)** Quantification of the Hec1-S55 phosphorylation in RPE-1 cells arrested in metaphase expressing Aurora A that cannot localize to the spindle. Relative intensity of the phospho-Hec1-S55 signal in cells treated as in D was calculated and displayed as in Fig. 2 B. The median of DMSO-treated cells was set as 1. The data represent a minimum of 105 kinetochores from five cells for each condition. P values were obtained using the Steel–Dwass multiple comparisons test. **(F)** Phosphorylation of Aurora A–T288 in RPE-1 cells expressing mCherry–Aurora A–WT, S155R, or K162R. Cells used in D were treated as in Fig. S3 A, fixed, and stained with anti–phospho–Aurora A–T288 (red) and anti-mCherry (green) antibodies. The mClover signal (blue) was acquired by fluorescence microscopy. Cells arrested in metaphase are shown. Scale bar: 5 µm. **(G)** Quantification of the Aurora A–T288 phosphorylation at spindle poles in RPE-1 cells expressing mCherry–Aurora A–WT, S155R, or K162R. Cells were treated as in F, and intensity

of the phospho–Aurora A–T288 signal against mCherry–Aurora A signal is shown. Error bars represent SD of a minimum of five cells for each condition. P values were obtained using the Dunnett's multiple comparisons test. **(H)** Aurora A distribution on the spindle in prometaphase (prometa) and metaphase. RPE-1 cells expressing Aurora A–mAID-mClover were fixed and stained with anti-GFP (mClover, green) and anti–α-tubulin (α-tub; red). DNA was stained with DAPI (blue). Scale bar: 5 µm. Intensities of Aurora A–mAID-mClover are plotted as in Fig. 3 F in the graphs on the right. BSD, blasticidin S deaminase; Dox, doxycycline; 3E, TPX2-F307E F334E F335E; N, N-terminal fragment (aa 1–43) of TPX2.

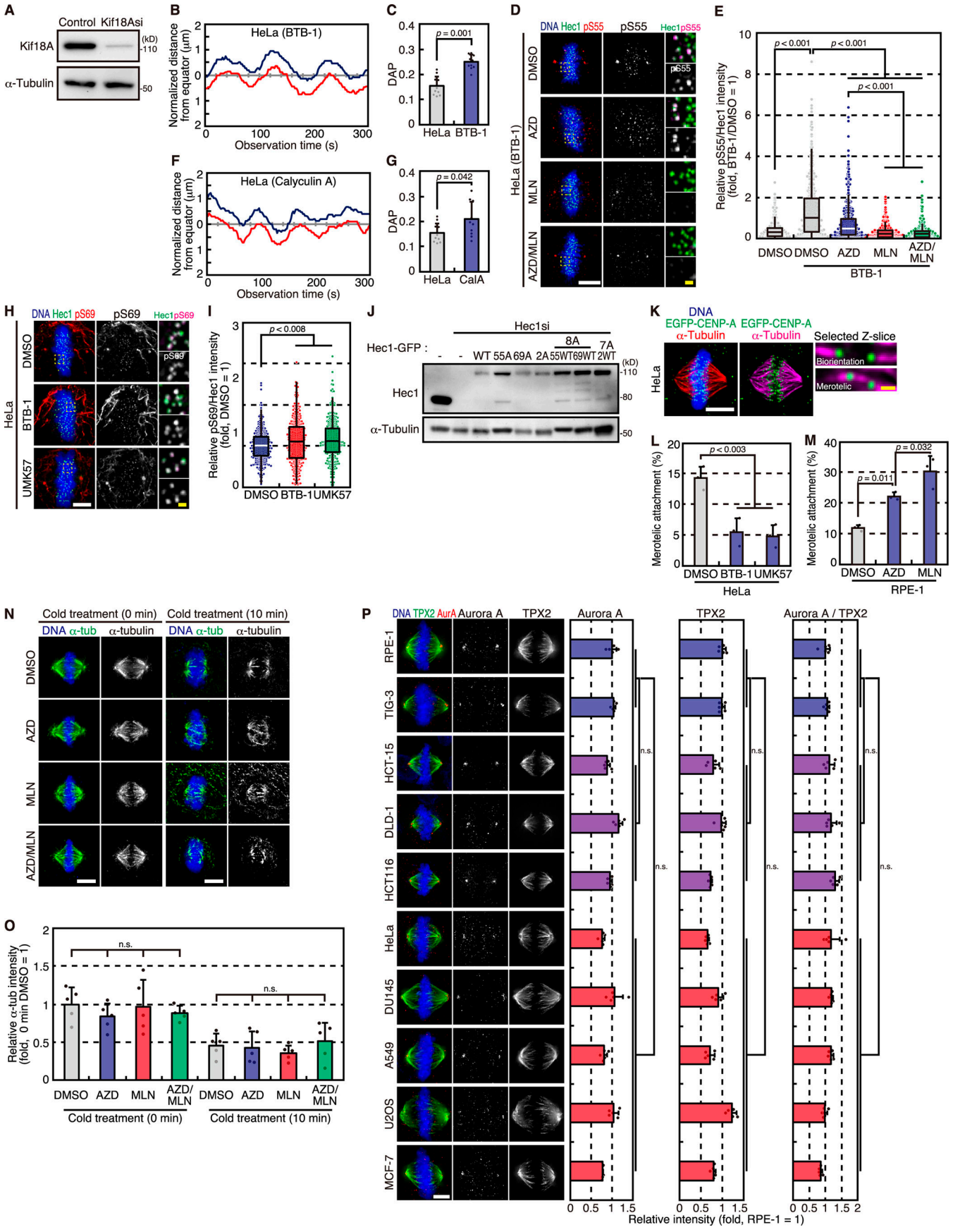

Figure S5. **Chromosome oscillation and the Aurora A–dependent Hec1 phosphorylation promote each other and facilitate the correction of erroneous kinetochore–microtubule attachments during metaphase. (A)** Efficiency of Kif18A RNAi. Lysate of cells transfected with an siRNA against Kif18A was subjected to immunoblot analysis using antibodies as indicated. **(B)** Trajectories of kinetochores in HeLa cells arrested in metaphase in the presence or absence of BTB-1, a Kif18A inhibitor. Cells were treated with or without BTB-1 for the last 1 h of a 2-h MG132 treatment and observed by live-cell imaging. The blue and red trajectories show the movements of a pair of sister kinetochores in cells treated with BTB-1 plotted as the distance from the spindle equator. See also Video 4. **(C)** DAP measurements of kinetochore position in HeLa cells treated as in B. Error bars represent SD of 10 kinetochore pairs from three cells. P value was obtained using the Student's *t* test. **(D)** Hec1-S55 phosphorylation in HeLa cells during metaphase in the presence of BTB-1. Cells were treated with BTB-1 and either DMSO or AZD1152 and/or MLN8237 for the last 1 h of a 3-h MG132 treatment, then fixed and stained with anti-Hec1 (green) and anti–phospho-Hec1-S55 (red) antibodies. DNA was stained with DAPI (blue). Cells arrested in metaphase are shown. Boxed regions in the panels are shown as magnified images in insets. Scale bar: 5 µm (white), 500 nm (yellow). **(E)** Quantification of the Hec1-S55 phosphorylation signal in HeLa cells treated as in D, which was calculated and displayed as box and dot plots as in Fig. 2 B. The median of cells treated with BTB-1 without Aurora inhibitors was set as 1. The data represent a minimum of 347 kinetochores from five cells for each condition. P values were obtained using the Steel–Dwass multiple comparisons test. **(F)** Trajectories of kinetochores in HeLa cells arrested in metaphase in the presence or absence of Calyculin A. Cells were treated with or without Calyculin A for the last 1 h of a 2-h MG132 treatment, then observed by live-cell imaging. The blue and red trajectories show the movements of a pair of sister kinetochores in cells treated with Calyculin A, plotted as the distance from the spindle equator. See also Video 5. **(G)** DAP measurements of kinetochore position in RPE-1 cells treated as in F. Error bars represent SD of 10 kinetochore pairs from three cells. P value was obtained using the Student's *t* test. **(H)** Hec1-S69 phosphorylation in HeLa cells during metaphase in the presence of BTB-1 or UMK57, a MCAK potentiator. Cells were treated with BTB-1 or UMK57 for the last 1 h of a 3-h MG132 treatment, then fixed and stained with anti-Hec1 (green) and anti–phospho-Hec1-S69 (red) antibodies. DNA was stained with DAPI (blue). Cells arrested in metaphase are shown. Boxed regions in the panels are shown as magnified images in insets. Scale bar: 5 µm (white), 500 nm (yellow). **(I)** Quantification of the Hec1-S69 phosphorylation signal in HeLa cells treated as in H, which was calculated and displayed as in Fig. 2 B. The median of DMSO-treated cells was set as 1. The data represent a minimum of 259 kinetochores from five cells for each condition. P values were obtained using the Steel multiple comparisons test. **(J)** Expression of Hec1 constructs in RPE-1 cells depleted of endogenous Hec1. Lysate of Hec1-depleted cells transfected with each Hec1 construct was subjected to immunoblot analysis using antibodies as indicated. **(K)** Kinetochore–microtubule attachments in metaphase HeLa cells. HeLa cells expressing EGFP–CENP-A were subjected to immunostaining with an antibody against GFP (green) and α-tubulin (red). DNA was stained with DAPI (blue). Magnified view of kinetochore–microtubule attachments in selected Z-slices are shown in insets, where merotelic attachment was judged by the presence of microtubules between sister kinetochores. Scale bar: 5 µm (white), 500 nm (yellow). **(L)** Quantification of the kinetochore pairs forming merotelic attachment in HeLa cells arrested in metaphase in the presence of BTB-1 or UMK57. HeLa cells expressing EGFP–CENP-A were fixed and stained as in K. The data represent the percentage of merotelic attachment, and error bars represent SD of three independent experiments in which a minimum of 100 kinetochore–microtubule attachments in a minimum of 10 cells were observed for each condition. P values were obtained using the Dunnett's multiple comparisons test. **(M)** Quantification of the kinetochore pairs in RPE-1 cells arrested in metaphase forming merotelic attachment in the presence of AZD1152 or MLN8237. RPE-1 cells expressing EGFP–CENP-A were fixed and stained as in K. The data represent the percentage of merotelic attachment, and error bars represent SD of three independent experiments in which a minimum of 100 kinetochore–microtubule attachments in a minimum of 10 cells were observed for each condition. P values were obtained using the Dunnett's multiple comparisons test. **(N)** Spindle morphology of RPE-1 cells treated with or without Aurora inhibitors. Cells were treated with either DMSO or AZD1152 and/or MLN8237 for the last 1 h of the 3-h MG132 treatment, then incubated on ice for 0 or 10 min before fixation and stained with an anti–α-tubulin antibody (α-tub; green). DNA was stained with DAPI (blue). Scale bars: 5 µm. **(O)** Quantification of microtubule signals on the spindle. The α-tubulin signal intensities on the spindle of cells treated as in N were measured. The intensity of DMSO-treated cells without cold treatment was set as 1. Error bars represent SD of a minimum of five cells for each condition. P values were obtained using the Tukey-Kramer multiple comparisons test. **(P)** Expression of Aurora A and TPX2 on the spindle in nontransformed and cancer cell lines during metaphase. Cells were treated with MG132 for 3 h and then fixed and stained with anti–Aurora A (AurA; red) and anti-TPX2 (green) antibodies. DNA was stained with DAPI (blue). Scale bar: 5 µm. Signal intensity of Aurora A and TPX2 and the signal ratio of Aurora A to TPX2 are shown in the right graphs. The average values in RPE-1 cells were set as 1. Error bars represent SD of five independent experiments in which a minimum of 10 cells were observed for each cell line. P value was obtained using the Tukey-Kramer multiple comparisons test.

Video 1. **Video of chromosome oscillation in RPE-1 and HeLa cells.** Images were taken every 2 s, and video speed is 20 frames per second (sec).

Video 2. **Video of chromosome motion in RPE-1 and HeLa cells in the absence of MG132.** Images were taken every 5 s, and video speed is 8 frames per second (sec).

Video 3. **Video of chromosome oscillation in TIG-3, HCT-15, DLD-1, HCT116, DU145, A549, U2OS, and MCF-7 cells.** Images were taken every 2 s, and video speed is 20 frames per second (sec).

Video 4. **Video of chromosome oscillation in an RPE-1 cell treated with taxol, a HeLa cell depleted of Kif18A, a HeLa cell treated with BTB-1, and a HeLa cell treated with UMK57.** Images were taken every 2 s, and video speed is 20 frames per second (sec).

Video 5. **Video of chromosome oscillation in an RPE-1 cell treated with AZD1152, an RPE-1 cell treated with MLN8237, an Aurora A–mAID-mClover–expressing RPE-1 cell treated with DMSO, an Aurora A–mAID-mClover–expressing RPE-1 cell treated with IAA, and a HeLa cell treated with Calyculin A.** Images were taken every 2 s, and video speed is 20 frames per second (sec).

Video 6. **Video of chromosome oscillation in an RPE-1 cell expressing Hec1-WT, Hec1-S55A, Hec1-S69A, Hec1-2A, Hec1-8A-S55WT, Hec1-8A-S69WT, or Hec1-7A-2WT depleted of endogenous Hec1.** Images were taken every 2 s, and video speed is 20 frames per second (sec).